Yeast Nst1 is a novel component of P-bodies and is a specific suppressor of proteasome base assembly defects

Chin Leng Cheng[a], Michael K. Wong[a], and Mark Hochstrasser[a,b,*]
[a]Department of Molecular Biophysics and Biochemistry and [b]Department of Molecular, Cellular, and Developmental Biology, Yale University, New Haven, CT 06520

ABSTRACT **Proteasome assembly utilizes multiple dedicated assembly chaperones and is regulated by signaling pathways that respond to diverse stress conditions. To discover new factors influencing proteasome base assembly, we screened a tiled high-copy yeast genomic library to identify dosage suppressors of a temperature-sensitive proteasome regulatory particle (RP) base mutant. The screen identified negative salt tolerance 1 (Nst1), a protein that when overexpressed specifically suppressed the temperature sensitivity and proteasome-assembly defects of multiple base mutants. Nst1 overexpression reduced cytosolic RP ATPase (Rpt) aggregates in *nas6*Δ *rpn14*Δ cells, which lack two RP assembly chaperones. Nst1 is highly polar and predicted to have numerous intrinsically disordered regions, characteristics commonly found in proteins that can segregate into membraneless condensates. In agreement with this, both endogenous and overexpressed Nst1 could form cytosolic puncta that colocalized with processing body (P-body) components. Consistent with the accumulation of translationally inactive mRNAs in P-bodies, Nst1 overexpression inhibited global protein translation in *nas6*Δ *rpn14*Δ cells. Translational inhibition is known to suppress aggregation and proteasome assembly defects in base mutants under heat stress. Our data indicate that Nst1 is a previously overlooked P-body component that, when expressed at elevated levels inhibits translation, prevents Rpt subunit aggregation and rescues proteasome assembly under stress conditions.**

Monitoring Editor
Anne Spang
University of Basel

Received: Apr 12, 2021
Revised: Jul 2, 2021
Accepted: Jul 27, 2021

INTRODUCTION

The 26S proteasome is a multi-subunit protease complex conserved in all eukaryotes (Tomko and Hochstrasser, 2013; Budenholzer *et al.*, 2017). The eukaryotic 26S proteasome is divided into three major subcomplexes: the core particle (CP), regulatory particle (RP) base, and RP lid. The RP base comprises six distinct AAA+ ATPases called RP ATPase (Rpt) Rpt1-Rpt6 and three non-ATPase subunits, Rpn1, Rpn2, and Rpn13. Rpn1,and Rpn13, together with Rpn10, are receptors for ubiquitin-modified substrates, while the Rpt1-Rpt6 subunits function to unfold and translocate these substrates into the proteolytic CP for degradation (Bard *et al.*, 2018). Due to the complexity of the RP base, its assembly is facilitated by several dedicated RP assembly chaperones (RACs): Hsm3, Nas2, Nas6, and Rpn14 and the more recently identified yeast-specific Adc17 (Funakoshi *et al.*, 2009; Kaneko *et al.*, 2009; Le Tallec *et al.*, 2009; Roelofs *et al.*, 2009; Saeki *et al.*, 2009; Hanssum *et al.*, 2014).

Proteasome assembly is affected by diverse stress conditions. When demand for proteasomes increases during proteotoxic stresses, Rpn4, a yeast transcriptional activator of proteasome subunit genes that is also a proteasome substrate, is stabilized and, as a result, up-regulates transcription of these genes by binding to proteasome-associated control elements (PACE) in their promoters

This article was published online ahead of print in MBoC in Press (http://www.molbiolcell.org/cgi/doi/10.1091/mbc.E21-04-0178).

*Address correspondence to: Mark Hochstrasser (mark.hochstrasser@yale.edu).

Abbreviations used: BME, β-mercaptoethanol; CP, core particle; eGFP, enhanced GFP; HRP, horseradish peroxidase; MAPK, mitogen-activated protein kinase; NST, negative salt tolerance; PACE, proteasome-associated control element; PONDR, Predictor of Naturally Disordered Regions; P-body, processing body; RAC, regulatory particle assembly chaperone; RP, regulatory particle; Rpt, regulatory particle ATPase; SD, selective defined; TCA, trichloroacetic acid; TORC1, target of rapamycin 1; ts, temperature sensitive; WT, wild type.

(Mannhaupt *et al.*, 1999; Xie and Varshavsky, 2001; Ju *et al.*, 2004; London *et al.*, 2004). In addition, expression of RACs is induced by stressors such as tunicamycin and rapamycin; this induction is regulated by the target of rapamycin 1 (TORC1) pathway (Rousseau and Bertolotti, 2016). Rapamycin inhibits TORC1 activity, which in turn activates the mitogen-activated protein kinase (MAPK) Slt2/Mpk1; activation of Slt2 is responsible for the up-regulation of RAC protein levels (Rousseau and Bertolotti, 2016).

In our study, we sought to determine if there were other chaperones or regulatory pathways that influence proteasome base assembly. To discover potential novel regulators of assembly, we conducted a suppressor screen to identify genes that in high dosage suppress the temperature-sensitive (ts) growth of a previously characterized base mutant, *rpt2,5PA*, in *Saccharomyces cerevisiae* (Cheng *et al.*, 2021). This strain has alanine substitutions for conserved proline residues located between the coiled-coil and oligonucleotide/oligosaccharide-binding domains in Rpt2 (P103) and Rpt5 (P76). These mutations result in increased aggregation of Rpt subunits and strong proteasome base assembly defects. One strong suppressor identified from the screen was *NST1* (negative salt tolerance 1), a poorly understood gene. Mutant *nst1* cells have a higher tolerance of high salt stress relative to wild-type (WT) strains (Goossens *et al.*, 2002), but how loss of *NST1* contributes to salt tolerance is unknown. In the same study, Nst1 was also found to bind splicing factor Msl1 (Goossens *et al.*, 2002). A more recent investigation reported that Nst1 binds Ste11 and Mkk1, components of separate MAPK pathways (HOG1 and CWI), potentially bridging these two pathways in response to heat stress (Leng and Song, 2016). In the latter study, deletion of *NST1* was found to delay phosphorylation of the MAP kinase Slt2 in cells subjected to high temperature (Leng and Song, 2016).

We investigated the basis of Nst1-facilitated suppression of the temperature sensitivity of *rpt2,5PA* and other yeast base mutants. Nst1 only suppressed the temperature sensitivity of mutants with RP base assembly defects. Overexpression of Nst1 also suppressed aggregation and cytosolic puncta formation of Rpt subunits in base mutants subjected to heat stress. Nst1 itself formed cytosolic foci, especially when expressed at high levels, but these did not colocalize with Rpt puncta. Surprisingly, Nst1 was instead found in processing bodies (P-bodies), which are membraneless cytoplasmic condensates containing translationally inactive mRNAs and proteins involved in translational control and mRNA decay (Luo *et al.*, 2018).

We found that endogenous Nst1 is a bona fide P-body component under specific stress conditions and characterized regions in Nst1 that are important for its localization and function. Nst1 overexpression inhibited bulk protein translation, and this translational repression is likely responsible for the suppression of the Rpt aggregation and growth defects of proteasome base mutants. In agreement with this, several known P-body components could similarly suppress these same base mutant deficiencies. Due to the highly charged and disordered nature of Nst1, we propose that Nst1 promotes the sequestration of untranslated mRNAs in P-bodies, contributing to global translation inhibition. This may reduce proteasome base subunit amounts in base mutant cells, thereby preventing their aggregation and rebalancing levels of proteasome assembly intermediates to promote their orderly assembly into complete RP base complexes.

RESULTS

Nst1 overexpression suppresses temperature sensitivity of proteasome base mutants

Using an ordered library of yeast genomic DNA-containing high-copy plasmids (Jones *et al.*, 2008), we identified a number of clones capable of suppressing the strong *rpt2,5PA* growth defect at elevated temperature (Table 1). As expected, we identified the WT *RPT2* and *RPT5* genes among these clones; we also identified multiple known RAC-encoding genes, validating the approach to identifying potential regulators of proteasome assembly with our screen. The strongest novel suppressor was *NST1*. We found that supplementary expression of *NST1* at both low and high levels partially suppressed temperature sensitivity of this mutant (Figure 1A).

To determine the specificity of suppression by *NST1*, we examined its ability to suppress various ts ubiquitin-proteasome system mutants. Remarkably, increased dosage of *NST1* exclusively suppressed ts mutations in the RP base or base assembly factors (Table 2; Supplemental Figure S1). In addition to *rpt2,5PA*, the strongest Nst1-driven suppression was observed with *cim3-1* (a mutant of Rpt6) and especially *nas6*Δ *rpn14*Δ (Figure 1B). Hence, we focused our subsequent Nst1 analysis on these three mutants. We note that increased levels of *NST1* expression often inhibited yeast growth, particularly at 30°C; this toxicity might overwhelm its suppressive capacity in some mutants.

Nst1 is a large protein (142 kDa) that is highly charged, with His, Lys, and Glu residues concentrated in its central region (Figure 1C). In addition, a conserved domain of 50–60 residues unique to Nst1 and its orthologs is located near the N-terminus (Figure 1C; discussed in next section) (Goossens *et al.*, 2002). Nst1 also contains a serine-rich region at the C-terminus of the protein. Using the Predictor of Naturally Disordered Regions (PONDR) program, we found that Nst1 likely contains many disordered regions, the largest of which is the central region rich in charged residues (Figure 1D) (Romero *et al.*, 2001).

We next created a series of Nst1 truncations, mostly removing C-terminal segments but also including one N-terminal truncation, $Nst1_{440\text{-}1240}$. The latter mutant removed the most conserved element in Nst1 and abrogated suppression of *nas6*Δ *rpn14*Δ temperature sensitivity (Figure 1E). The C-terminal truncation analysis revealed that any truncation past the serine-rich region was sufficient to inhibit growth rescue by the overexpressed Nst1 mutant, suggesting the importance of this polar region for Nst1 function (Figure 1E). Interestingly, protein expression analysis of these truncation mutants revealed that levels of the Nst1 C-terminal truncations that no longer could suppress *nas6*Δ *rpn14*Δ were expressed at much higher levels than either WT Nst1-FLAG or the still functional $Nst1_{1\text{-}1170}$-FLAG; the latter was expressed at lower than WT levels, consistent with its reduced efficiency in suppressing the temperature sensitivity of *nas6*Δ *rpn14*Δ cells. N-terminally truncated $Nst1_{440\text{-}1240}$-FLAG was expressed at similar levels to the WT protein (Figure 1F). Taken together, our findings highlight the functional importance of both the N-terminal region, which includes the Nst1 domain, and the C-terminal serine-rich region, which is also important for the regulation of Nst1 protein levels.

The Nst1 domain is a distinguishing feature of Nst1 orthologs in diverse species

Sequence analysis of Nst1 identified a well-conserved N-terminal domain of ~50–60 residues that had been denoted as the "Nst1 domain" (Figure 1C) (Goossens *et al.*, 2002). Using the Nst1 domain for sequence homology searches, we discovered that Nst1 is conserved not only in ascomycetes as previously predicted (Goossens *et al.*, 2002) but is also widespread in basidiomycetes. Outside of *Fungi*, we found Nst1 homologues in several *Amoebozoa* and in different multicellular green algal charophyte species, which are thought to be related to land plant progenitors; examples were also found in *Naegleria* (Excavata) and a handful of bacteria and other

Clone	Replicates										
YGPM10d08	2	YML003W	YML002W	YPT7	[CDC5]&						
YGPM14n17	2	[YBR271W]&	HSM3	UBX7	CHK1	RIF1	[PPS1]&				
YGPM29h14	1	[PWP2]*	YIH1	TAH1	YCR061W	tS(CGA)C	YCR064C	BUD31	HCM1	RAD18	[SED4]&
YGPM17a22	1	[KAP120]&	[SPC29]	RNY1	TFB2	MEI5	VPS30	YPL119C-A	DBP1	MRP51	IDI1
YGPM2h16	1	[YGL006W-A]	PMC1	COG7	RPN14	CDH1	ERP6	[ERG26]&			
YGPM31b14	1	[SCY1]&	YGL082W	YGL081W	FMP37	YGL079W	DBP3	HNM1	[RPL7A]&		
YGPM29g19	2	[FAA3]&	URM1	NAS2	YIL006W	EPS1	BET1	CFD1	YIL002W-A	[INP51]&	
YGPM4n12	1	[BAR1]	tD(GUC)I1	YIL014C-A	tT(AGU)I2	MNT3	[PDR11]				
YGPM23l22	1	[PDR11]*	YIL012W	TIR3	DOT5	EST3	tD(GUC)I2	FAA3	URM1	[NAS2]&	
YGPM7f11	1	[PUT3]&	URB1	ARC19	PRP40	[CCE1]	[UFD4]&				
YGPM4d21	1	[TAL1]*	ILV5	YLR356W	RSC2	YLR358C	ADE13				
YGPM5d16	1	[YML002W]&	YPT7	CDC5	YMR001C-A	YMR002W	YMR003W	[MVP1]*			
YGPM7e18	2	[YNL092W]	NST1	RHO2	YNL089C	[TOP2]*					
YGPM13d08	5	[YOR114W]	TRS33	RPO31	RPT5	[YOR118W]*					
YGPM33m13	4	[RPO31]*	RPT5	YOR118W	RIO1	GCY1	YOR121C	PFY1	LEO1	[UBP2]&	
YGPM12f20	2	[HAT1]&	CIT3	PDH1	tF(GAA)P1	YPR002C-A	YPR003C	[YPR004C]&			
YGPM16j22	8	[YDL011C]*	[YDL010W]&	YDL009C	APC11	tT(AGU)D	tS(AGA)D1	RPT2	PTC1	[MED2]&	

NST1 is highlighted in yellow, base assembly chaperone genes are highlighted in blue, and *RPT2* and *RPT5* are highlighted in green. The isolation of these suppressor plasmids, many of which contain *RPT2* and *RPT5*, serves as positive controls for the screen. Bracketed genes with * and & contain 5′-end and 3′-end truncations, respectively.

TABLE 1: Suppressor hits from two rounds of screen.

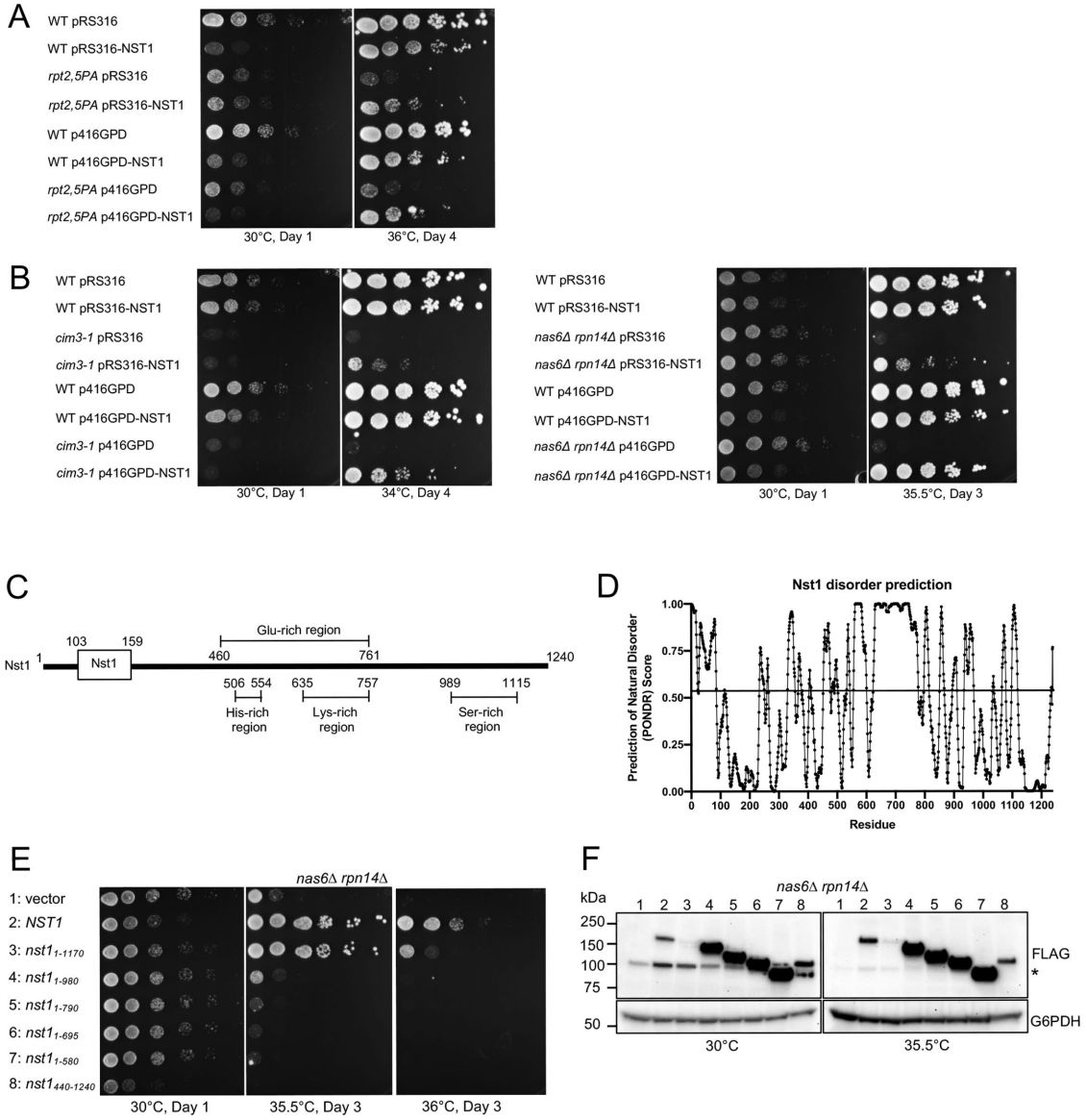

FIGURE 1: Overexpression of Nst1 suppresses growth defects of proteasome base mutants. (A) WT and *rpt2,5PA* cells were transformed with pRS316 (empty vector), pRS316-NST1, p416GPD (empty vector), or p416GPD-NST1. Cells were spotted on SD-URA plates. (B) WT and *cim3-1* cells and WT and *nas6*Δ *rpn14*Δ strains were transformed with the indicated plasmids. Cells were spotted on SD-URA plates. (C) Analysis of composition and sequence features of *S. cerevisiae* Nst1. (D) Nst1 disorder prediction from PONDR. Higher PONDR scores indicate greater likelihood of disorder. Several regions of Nst1, including the highly charged central region, are predicted to be intrinsically disordered. (E) Growth suppression analysis of overexpressed Nst1 truncation mutants in *nas6*Δ *rpn14*Δ. Yeast *nas6*Δ *rpn14*Δ cells were transformed with plasmid (p416GPD) expressing the indicated *NST1* derivatives. All expressed proteins were tagged with FLAG at the C-terminus. Cells were spotted on SD-URA plates. (F) Analysis of protein levels of Nst1 truncation mutants. Overnight cultures of each strain were diluted to OD_{600} = 0.2 in SD-URA and grown at either at 30°C or 35.5°C to midexponential phase. All constructs were FLAG-tagged at the C-terminus and expressed in the p416GPD vector as in E. Lanes 1, vector; 2, Nst1; 3, $Nst1_{1\text{-}1170}$; 4, $Nst1_{1\text{-}980}$; 5, $Nst1_{1\text{-}790}$; 6, $Nst1_{1\text{-}695}$; 7, $Nst1_{1\text{-}580}$; 8, $Nst1_{440\text{-}1240}$. *~100 kDa yeast protein recognized by anti-FLAG antibody.

species where its presence might reflect lateral gene transfer (Figure 2A; Supplemental Figure S2). Most of these Nst1-related proteins contain not only an N-terminal Nst1 domain but also a highly charged central region and are similar in size to scNst1 (Supplemental Figure S2).

When comparing the Nst1 domains of Nst1-like proteins from 926 different species (mostly fungi), four residues were found to be particularly well conserved: W103, C135, C137, and C140 (*S. cerevisiae* numbering; Figure 2B) (Thomsen and Nielsen, 2012). Interestingly, structural modeling of the scNst1 domain on the Phyre2 web portal (Kelley *et al.*, 2015) predicted structural similarity to a bacterial heat shock protein, Hsp33, which contains four absolutely conserved cysteines that are important for its function (Winter and Jakob, 2004; Kelley *et al.*, 2015). These cysteines coordinate a Zn^{2+} ion in the inactive form but become disulfide bonded under oxidative stress, creating a partially active protein. Two partially active Hsp33 monomers dimerize under heat stress to form a fully active chaperone (Winter and Jakob, 2004). A previous study has shown that the

Mutant strains	Description	Low-dosage *NST1*	High-dosage *NST1*
uba1-ts	E1 enzyme	No	No
sis1-ts	Type II HSP40 cochaperone	No	No
rpn12-234Δ	Lid subunit	No	No
sem1Δ	Lid subunit	No	No
pre9Δ	CP subunit	No	No
rpt1-ts (*cim5-1*)	Base subunit	No	No
rpt4-ts (*rpt4-G106D*)	Base subunit	Yes (weak suppression)	No
rpt6-ts (*cim3-1*)	Base subunit	Yes	Yes
rpt2,5PA	Base subunit	Yes	Yes
ump1Δ	CP chaperone	No	No
nas6Δ rpn14Δ	Base chaperones	Yes	Yes
hsm3Δ nas2Δ	Base chaperones	No	Yes (weak suppression)
nas6Δ rpn14Δhsm3Δ nas2Δ	Base chaperones	No	Yes

Strains with the genotypes listed were transformed with pRS316, pRS316-NST1 (low dosage), p416GPD, or p416GPD-NST1 (high dosage). Spot assays were conducted on SD-URA plates (see Supplemental Figure S1).

TABLE 2: Analysis of growth suppression by *NST1* overexpression (at low and high dosages) in various ts mutants.

nst1Δ strain is sensitive to heat stress (Leng and Song, 2016), which we confirmed. Interestingly, we found *nst1Δ* cells were also sensitive to diamide treatment, which specifically induces disulfide stress (Figure 2C). However, simultaneous mutation of all three conserved Nst1 domain cysteine residues did not inhibit the ability of the mutant strain to tolerate diamide stress (Figure 2D). Hence, the significance of the putative Hsp33 structural similarity for the newly discovered role of Nst1 in oxidative stress resistance remains to be determined.

Overexpressed Nst1 domain mutants were also tested for their ability to suppress the temperature sensitivity of *nas6Δ rpn14Δ* (Figure 2E). Removal of the Nst1 domain ($Nst1_{165\text{-}1240}$) or mutation of its most conserved residue (Nst1-W103A) strongly interfered with suppression. The cysteine mutations, however, did not. Expression levels of these mutants were similar to those of WT Nst1 except the $Nst1_{165\text{-}1240}$ protein (and Nst1-W103A at 30°C), which was present at higher levels (Figure 2F). Inactivation of Nst1 might lead to increases in its own expression, possibly by shielding the *NST1* mRNA from translational repression (see below).

Nst1 overexpression enhances proteasome assembly in RP base mutants

To determine if Nst1-mediated suppression of base mutant growth defects was due to improved proteasome assembly, we employed native immunoblot analysis. Although the effect was partial, Nst1 overexpression reproducibly increased levels of full 26S proteasomes in *nas6Δ rpn14Δ* and decreased levels of Blm10-CP complexes and assembly intermediates such as Rpt4-Rpt5 and free lid at elevated temperature (Figure 3A). The relative increase in levels of doubly and singly capped proteasomes and decrease in levels of Blm10-CP and CP complexes were also observed by proteasome activity measurements using fluorogenic substrate native gel-overlay assays (Figure 3, B and C). Nst1 overexpression also modestly suppressed the proteasome assembly defects in *rpt2,5PA* cells at nonpermissive temperature (Supplemental Figure S3). These data suggest that up-regulation of proteasome assembly contributes to the suppression of growth defects in these mutants.

Next, we determined the effects of *NST1* deletion on growth and proteasome assembly in different base mutants. *NST1* deletion showed moderate synthetic growth defects with *rpt2,5PA* and *cim3-1* (*rpt6-1*) and a very slight synthetic defect with *nas6Δ rpn14Δ* (Figure 3D). Native immunoblot analyses of these strains revealed that *nst1Δ* slightly exacerbated proteasome assembly defects of *rpt2,5PA* and *cim3-1* mutants but had little or no effect on *nas6Δ rpn14Δ* (Supplemental Figure S4, A–C). *NST1* deletion in *rpt2,5PA* and *cim3-1* mutants did not display an obvious decrease in full proteasomes but caused increases in several proteasome subcomplexes and intermediates such as CP, Blm10-CP, lid, and Rpn12 monomer (Supplemental Figure S4, A and B). Additionally, *NST1* deletion substantially decreased levels of the Rpt4-Rpt5 intermediate in *cim3-1* and *rpt2,5PA*. We observed a unique Rpt5-containing species from *cim3-1 nst1Δ* cells that could potentially be an off-pathway intermediate formed when Nst1 is absent (Supplemental Figure S4B). From these results, we infer that Nst1 is important in maintaining proper base assembly in mutant strains expressing defective Rpt subunits under proteotoxic stress.

Nst1 overexpression suppresses Rpt subunit aggregation in *nas6Δrpn14Δ*

We next asked whether the rescue of proteasome assembly and growth observed when Nst1 was overexpressed in RP base mutants could be attributed to up-regulation of base subunits and/or assembly chaperones. Nst1 was previously implicated in bridging two MAPK pathways (Leng and Song, 2016), and one of the pathways involves Slt2/Mpk1 kinase, an activator of base assembly chaperone expression under stress (Leng and Song, 2016; Rousseau and Bertolotti, 2016). However, Nst1 overexpression did not enhance levels of the tested proteasome subunits (Figure 4, A and B). Levels of the Hsm3, Nas2, and Nas6 RACs also appeared unaffected in WT and mutant strains overexpressing Nst1.

As in the *nas6Δ rpn14Δ* mutant, Nst1 overexpression failed to increase overall levels of Rpt subunits in *rpt2,5PA* cells, and levels of CP and lid subunits were also unaffected (Supplemental Figure S5, A and B). Notably, however, the soluble protein levels of several Rpt subunits were elevated by high Nst1 in this RP mutant, which we explore below. Both total and soluble Rpt4 levels were increased by Nst1 overexpression (Supplemental Figure S5); we speculate that this could be due to selective Rpt4 degradation in *rpt2,5PA* when

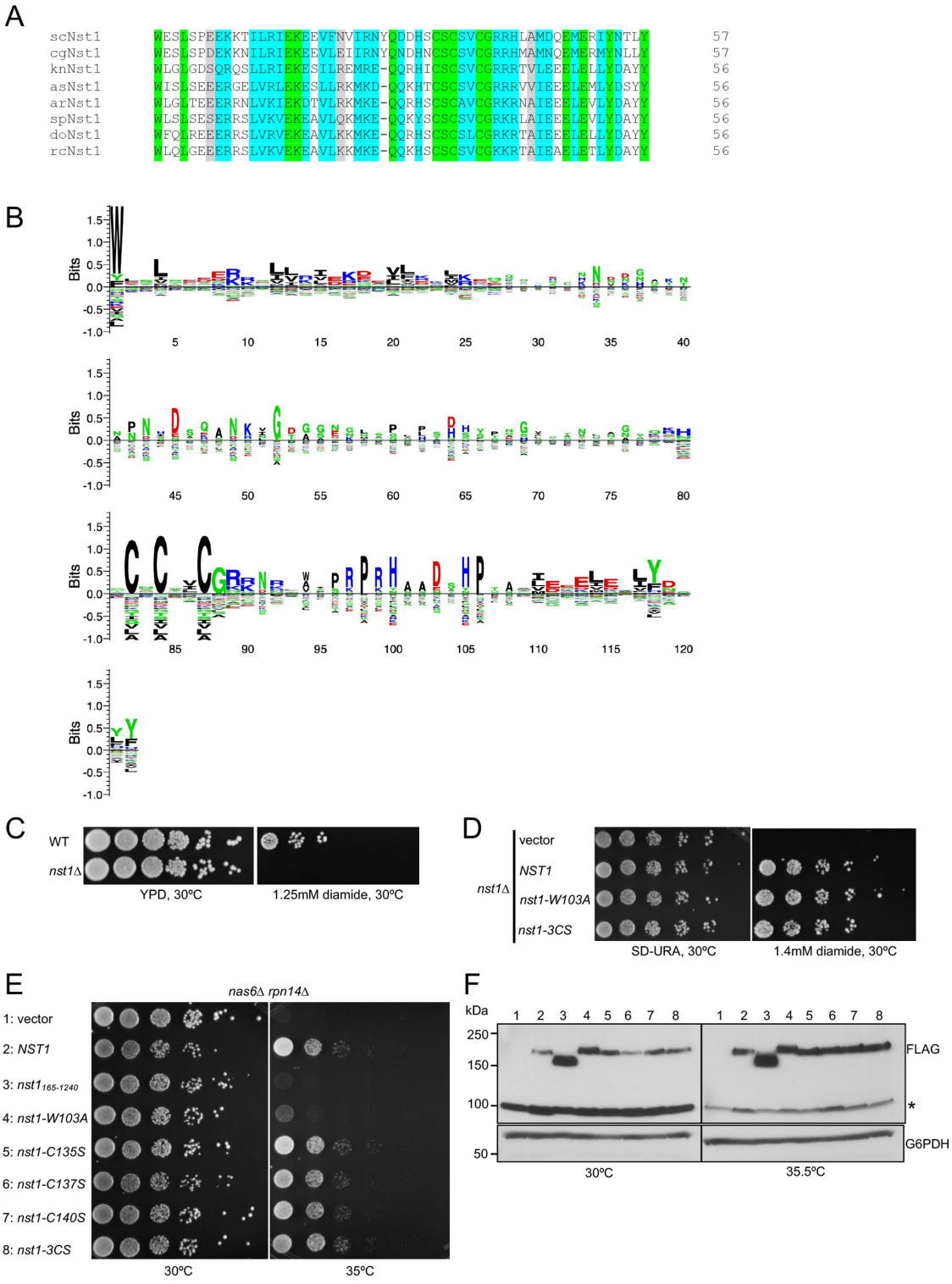

FIGURE 2: Conserved Nst1 domain identifies Nst1 orthologs in diverse species. (A) Multiple sequence alignment of Nst1 domain in diverse species. Sequence alignments conducted with the Clustal Omega (EMBL-EBI) alignment tool (green: complete conservation of residue; cyan: conserved residues with highly similar properties; gray: conserved residues with moderately similar properties). Abbreviations: *S. cerevisiae* (sc), *Candida glabrata* (cg), *Klebsormidium nitens* (kn), *Acytostelium subglobosum* (as), *Amanita rubescens* (ar), *Schizosaccharomyces pombe* (sp), *Dissophora ornata* (do), *Rhizophagus clarus* (rc). (B) Sequence logo plot illustrating the conservation of amino acids in Nst1 domain from various organisms. Nst1 domain sequences were first aligned using the Clustal Omega (EMBL-EBI) alignment tool, and the logo plot was created with Seq2Logo 2.0 (DTU Bioinformatics) using the default options. (C) Growth assay for diamide sensitivity. (D) The *nst1*Δ strain was transformed with either pRS316, pRS316-NST1-eGFP, pRS316-nst1-W103A-eGFP, or pRS316-nst1-3CS-eGFP in which the *NST1* variants were expressed using the native *NST1* promoter. 3CS: C135S, C137S, C140S triple mutant. (E) Growth suppression analysis of overexpressed Nst1 domain mutants in *nas6*Δ

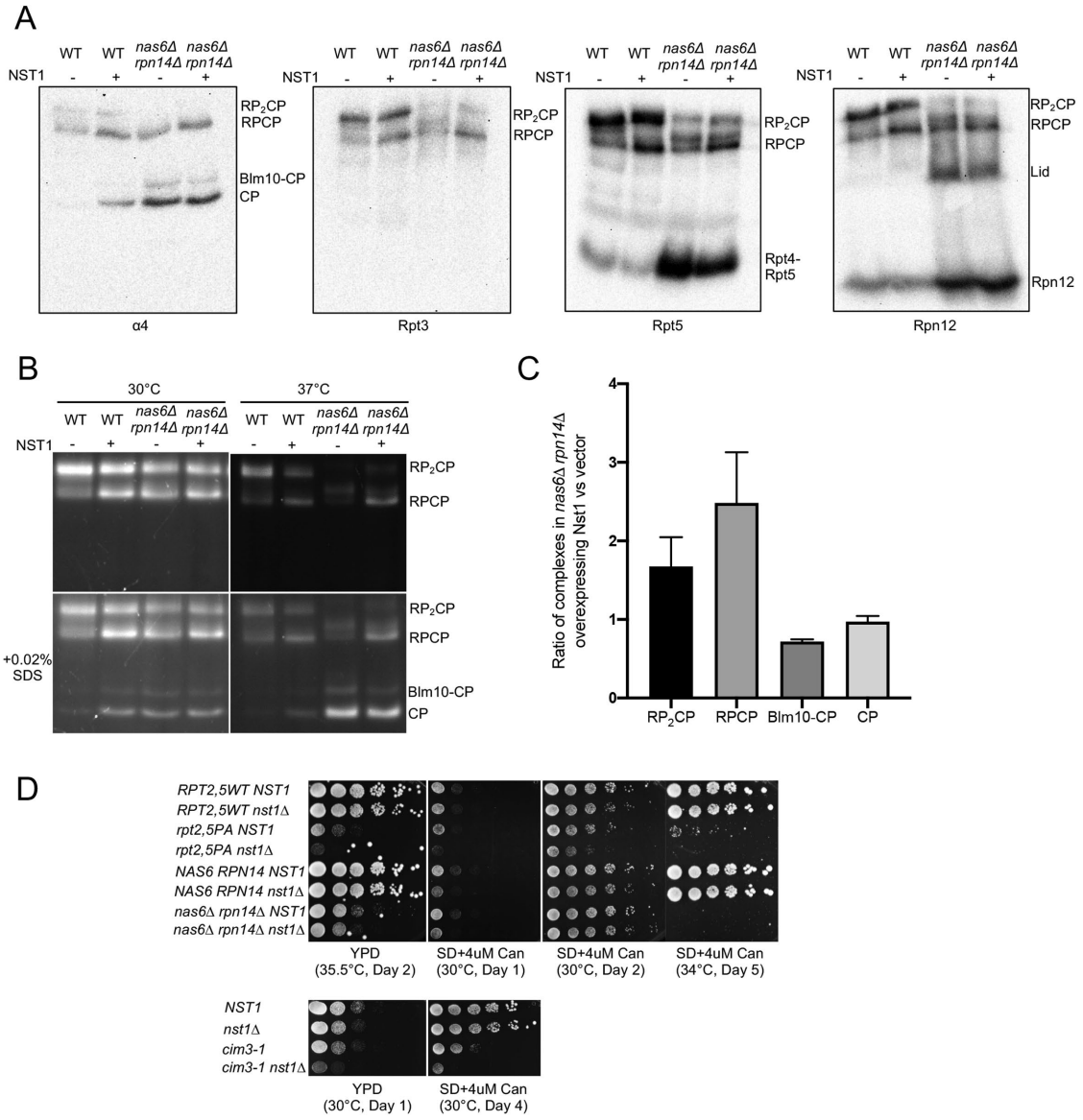

FIGURE 3: Nst1 overexpression enhances proteasome assembly in *nas6Δ rpn14Δ* cells at elevated temperature. (A) Western blot analyses of yeast whole cell extracts separated by nondenaturing-PAGE. WT and *nas6Δ rpn14Δ* strains were transformed with either p416GPD or p416GPD-NST1. Overnight cultures of each strain were diluted to OD_{600} = 0.2 in SD-URA and grown at 30°C for 2 h followed by another 3 h at 37°C. All strains express Rpt6 tagged with GFP at the N-terminus. (B) Suc-LLVY-AMC substrate overlay assay. WT and *nas6Δ rpn14Δ* cells were transformed with either p416GPD or p416GPD-NST1. Overnight cultures of each strain were diluted to OD_{600} = 0.2 in SD-URA and grown at 30°C for 2 h followed by another 3 h either at 30°C or at 37°C. Yeast whole cell extracts were resolved by nondenaturing-PAGE followed by overlay with the Suc-LLVY-AMC fluorogenic substrate. Activity of proteasomes was visualized with a UV transilluminator. The addition of 0.02% SDS activates free 20S CP in the gel. (C) Quantification of the Suc-LLVY-AMC-derived fluorescence intensity ratio of the indicated complexes in *nas6Δ rpn14Δ* cells transformed with p416GPD-NST1 to that of the same cells transformed with the empty p416GPD vector when freshly diluted cultures were grown at 30°C for 2 h followed by another 3 h at 37°C. Mean ± SD from three independent transformants each. (D) Yeast growth analysis of *nst1Δ* in combination with *nas6Δ rpn14Δ*, *rpt2,5PA*, or *cim3-1* mutations.

rpn14Δ. Mutant *nas6Δ rpn14Δ* cells were transformed with plasmid (p416GPD) overexpressing the indicated Nst1 constructs. All expressed proteins were FLAG-tagged at the C-terminus. Cells were spotted on SD-URA plates. (F) Analysis of protein levels of Nst1 truncation mutants. Overnight cultures of each strain were diluted to OD_{600} = 0.2 in SD-URA and grown at either at 30°C or 35.5°C until midexponential phase. All constructs were FLAG-tagged at the C-terminus and expressed in p416GPD vector as in E. Lanes 1, vector; 2, Nst1; 3, $Nst1_{165\text{-}1240}$; 4, Nst1-W103A; 5, Nst1-C135S; 6, Nst1-C137S; 7, Nst1-C140S; 8, Nst1-3CS. *~100 kDa yeast protein recognized by anti-FLAG antibody.

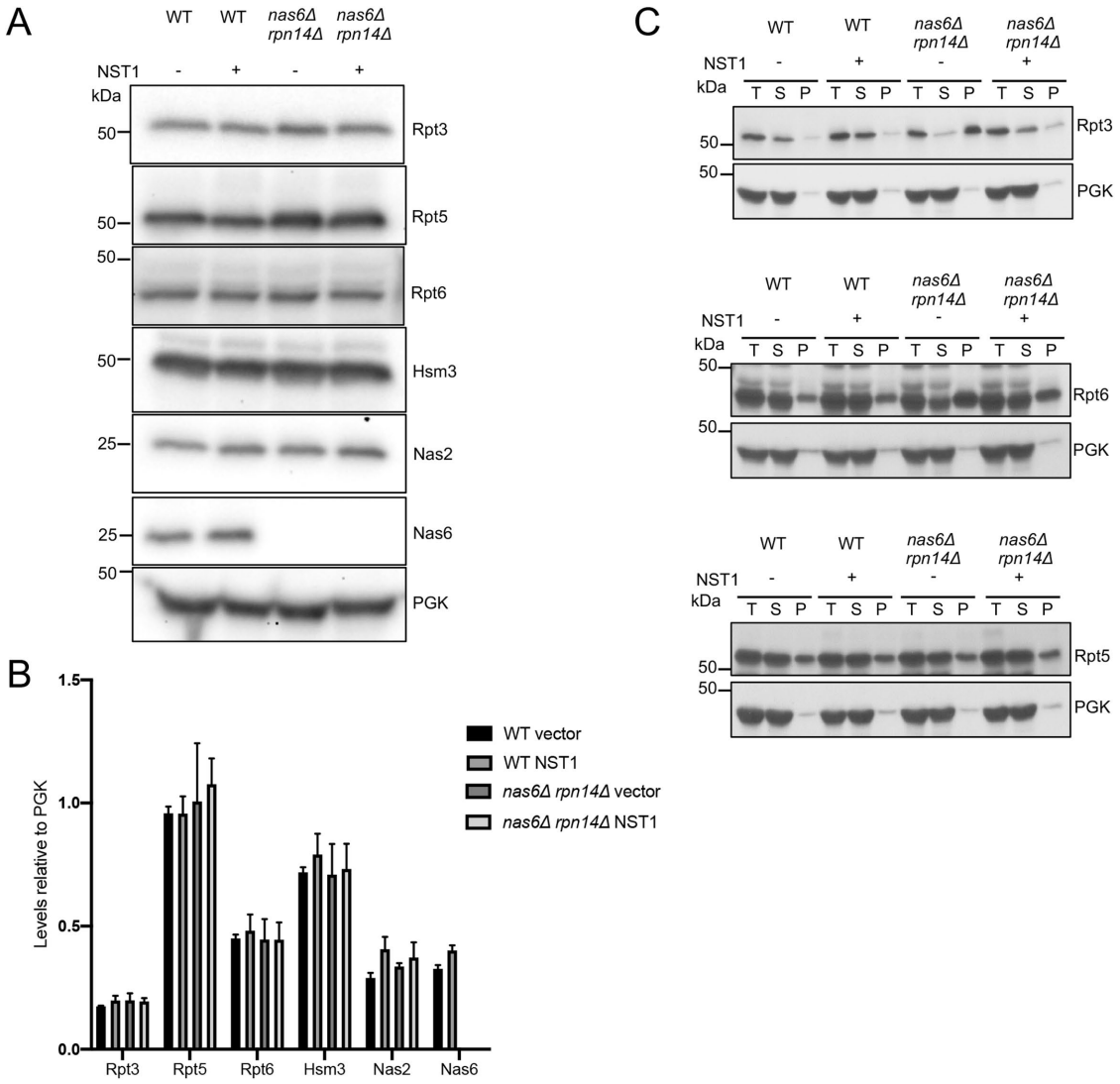

FIGURE 4: Nst1 overexpression inhibits aggregation of Rpt3 and Rpt6 in *nas6Δ rpn14Δ*. (A) Overall levels of proteasome subunits and RACs. Strains were transformed with either p416GPD or p416GPD-NST1. Overnight cultures were diluted to $OD_{600} = 0.2$ in SD-URA and grown at 30°C for 2 h followed by another 3 h at 37°C. Proteins were resolved by SDS–PAGE and immunoblotted with the indicated antibodies. (B) Quantification of proteasome subunits and chaperones levels. Mean ± SD from three independent transformants. (C) Aggregation analysis of Rpt3, Rpt5, and Rpt6 subunits. Cultures were grown as in (A). T, total protein; S, supernatant; P, pellet (100,000 × *g* for 20 min). Immunoblot analysis was performed with the indicated antibodies.

grown at nonpermissive temperature because soluble levels of its dimerization binding partner, Rpt5, are reduced in this mutant (Cheng *et al.*, 2021). Finally, we also found that overexpression of Nst1 in *rpt2,5PA* did not result in elevation of mRNA levels of proteasome subunits and chaperones (Supplemental Figure S6).

The enhancement of Rpt subunit solubility without effects on overall levels of these proteins in *rpt2,5PA* cells prompted the hypothesis that high Nst1 levels could limit aggregation of Rpt subunits in base assembly mutants. To test this, we conducted aggregation assays to determine if Nst1 overexpression influenced the aggregation status of Rpt subunits in *nas6Δ rpn14Δ* cells. Based on their relative levels in supernatant (S) and pellet (P) fractions, Rpt3 and Rpt6 aggregation was reduced to ~WT levels upon Nst1 overexpression in *nas6Δ rpn14Δ* cells (Figure 4C). Interestingly, aggregation of Rpt5 was not affected by Nst1 overexpression either in WT or in *nas6Δ rpn14Δ* cells, suggesting that Nst1 might selectively enhance the solubility of certain proteasome components. By contrast, overexpression of Nst1-W103A, $Nst1_{165\text{-}1240}$, and $Nst1_{1\text{-}980}$ failed to reduce aggregation of Rpt3 and Rpt6 in *nas6Δ rpn14Δ* (Supplemental Figure S7A). This is consistent with the inability of these mutants to suppress the temperature sensitivity of *nas6Δ rpn14Δ* cells (Figures 1E and 2E).

Nst1 overexpression suppresses puncta formation of Rpt1 and Rpt6 in *nas6Δrpn14Δ*

To visualize aggregates of Rpt subunits in *nas6Δ rpn14Δ* cells in vivo, we utilized a *nas6Δ rpn14Δ* mutant expressing endogenously tagged GFP-Rpt1 or GFP-Rpt6 subunits in the presence or absence of overexpressed Nst1 and tracked them by fluorescence microscopy. As previously reported, these Rpt subunits form cytosolic puncta when cells are under heat stress (Nahar *et al.*, 2019). Strikingly, the number of puncta was strongly suppressed when Nst1 was present at high levels (Figure 5A; Supplemental Figure S8). The size of the GFP-Rpt6 puncta, when present, was also generally smaller in

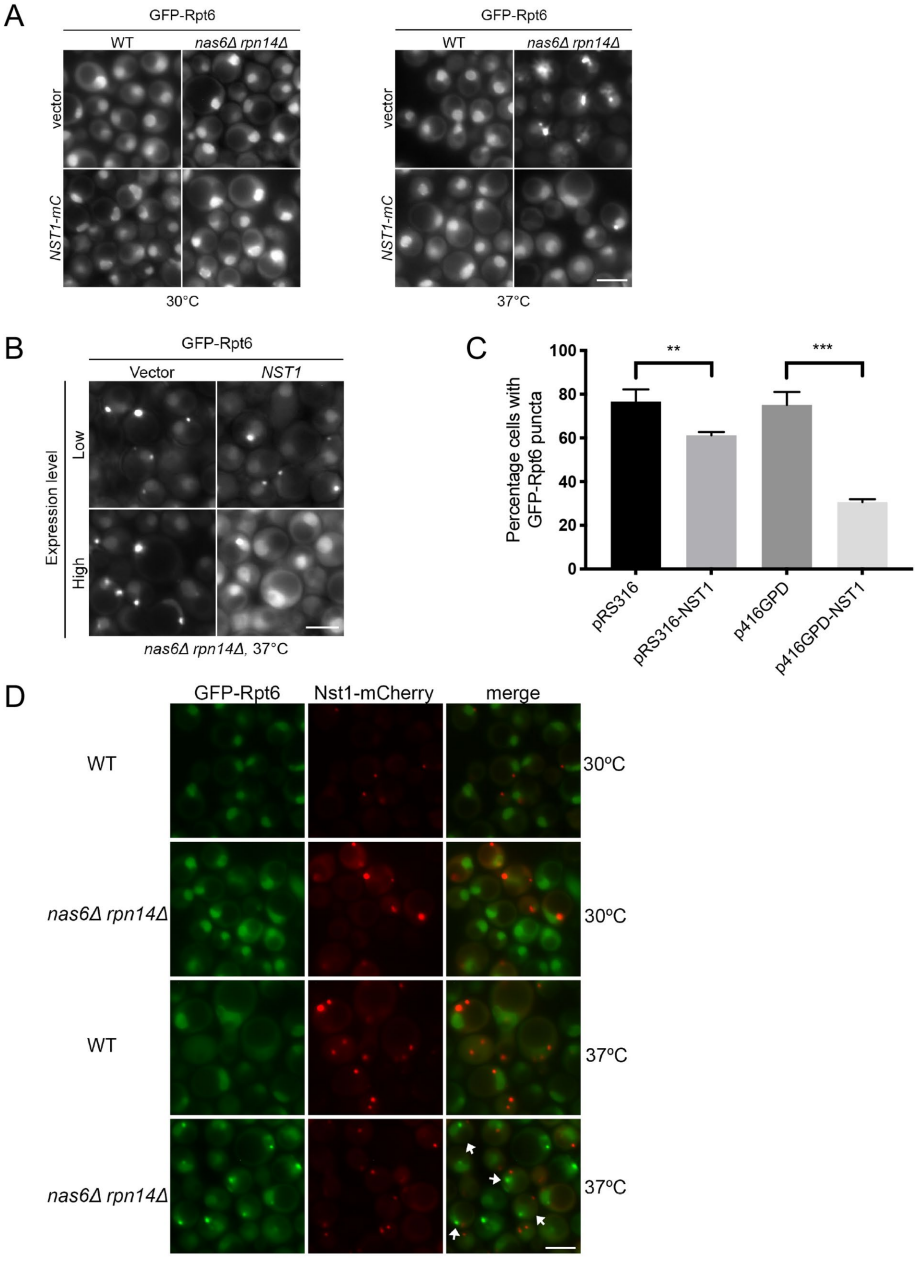

FIGURE 5: Rpt puncta formation is suppressed in *nas6*Δ *rpn14*Δ overexpressing Nst1. (A) Effect of Nst1-mCherry (mC) overexpression on GFP-Rpt6 puncta formation in *nas6*Δ *rpn14*Δ. WT and *nas6*Δ *rpn14*Δ cells with chromosomal *RPT6* tagged with *GFP* were transformed with p416GPD or p416GPD-NST1-mC. Overnight cultures of each strain were diluted to OD_{600} = 0.2 in SD-URA and grown for 2 h at 30°C followed by either 3 h at 30°C or 3 h at 37°C. GFP-Rpt6 distribution was visualized by fluorescence microscopy. (B) Effect of low and high Nst1 overexpression on GFP-Rpt6 puncta formation. The *nas6*Δ *rpn14*Δ mutant with chromosomally tagged *GFP-RPT6* was transformed with pRS316 or pRS316-NST1 for low-dosage analysis and p416GPD or p416GPD-*NST1* for high-dosage analysis. Cultures were diluted to OD_{600} = 0.2 in SD-URA and grown for 2 h at 30°C followed by 3 h at 37°C. GFP-Rpt6 was imaged by fluorescence microscopy. (C) Quantification of GFP-Rpt6 puncta formation in B. Mean ± SD from three independent transformants. More than 200 cells were analyzed for each isolate. Significance was measured by unpaired *t* test; $^{**}P < 0.01$; $^{***}P < 0.001$. (D) Nst1-mCherry and GFP-Rpt6 do not colocalize. Cultures were grown as in A. Arrows highlight cells containing both Nst1-mC and GFP-Rpt6 puncta. This field was chosen because it contains a higher number of GFP-Rpt6 foci than average to highlight the absence of colocalization between GFP-Rpt6 and Nst1-mCherry foci. Scale bar: 5 μm.

*nas6*Δ *rpn14*Δ overexpressing Nst1. The reduction in puncta formation was dependent on the degree of Nst1 overexpression, with greater reduction at higher expression of Nst1 (Figure 5, B and C). Overall, these microscopy data on Rpt6 puncta are consistent with our aggregation assays (Figure 4C). In contrast to WT Nst1 overexpression, Nst1-W103A, $Nst1_{165\text{-}1240}$, and $Nst1_{1\text{-}980}$ overexpression in *nas6*Δ *rpn14*Δ cells showed only a slight decrease in the number of cells containing GFP-Rpt6 puncta (Supplemental Figure S7, B and C).

It is noteworthy that overexpressed Nst1 tagged with mCherry could also form cytosolic puncta in WT and *nas6*Δ *rpn14*Δ cells at both 30˚C and 37˚C (Figure 5D). However, Nst1-mCherry and GFP-Rpt6 puncta did not colocalize. This suggests that Nst1-mediated suppression of Rpt aggregation is unlikely to occur via direct interactions between these proteins.

Nst1 localizes to P-bodies and can induce P-body assembly

Nst1 has characteristics of proteins that are able to undergo liquid–liquid phase separation (Boeynaems *et al.*, 2018). Such phase separation in the cell allows sequestration of toxic materials, clustering and enhancement of biochemical activity, or storage of cell components during stress conditions; these membraneless compartments are typified by P-bodies and stress granules (Boeynaems *et al.*, 2018). Both P-bodies and stress granules are ribonucleoprotein particle-containing granules implicated in mRNA storage, degradation, and translational repression (Decker and Parker, 2012). Previous genome-scale surveys suggested that Nst1 could physically interact with several P-body components such as Lsm4 and components of the Ccr4-Not deadenylase complex, although none of these Nst1 interactions had been validated (Fromont-Racine *et al.*, 2000; Uetz *et al.*, 2000; Tarassov *et al.*, 2008; Schlecht *et al.*, 2012). Multiple components of the Ccr4-Not complex localize to P-bodies (Muhlrad and Parker, 2005; Teixeira and Parker, 2007). Dhh1, a DEAD-box helicase and another P-body component, was found to interact with *NST1* mRNA based on high-throughput surveys (Jungfleisch *et al.*, 2017; Miller *et al.*, 2018).

Overexpressed Nst1-mCherry localized to P-bodies based on its colocalization with known P-body components Dcp2, Edc3, and Dhh1 (all tagged with GFP) under normal growth conditions (Figure 6A). On the

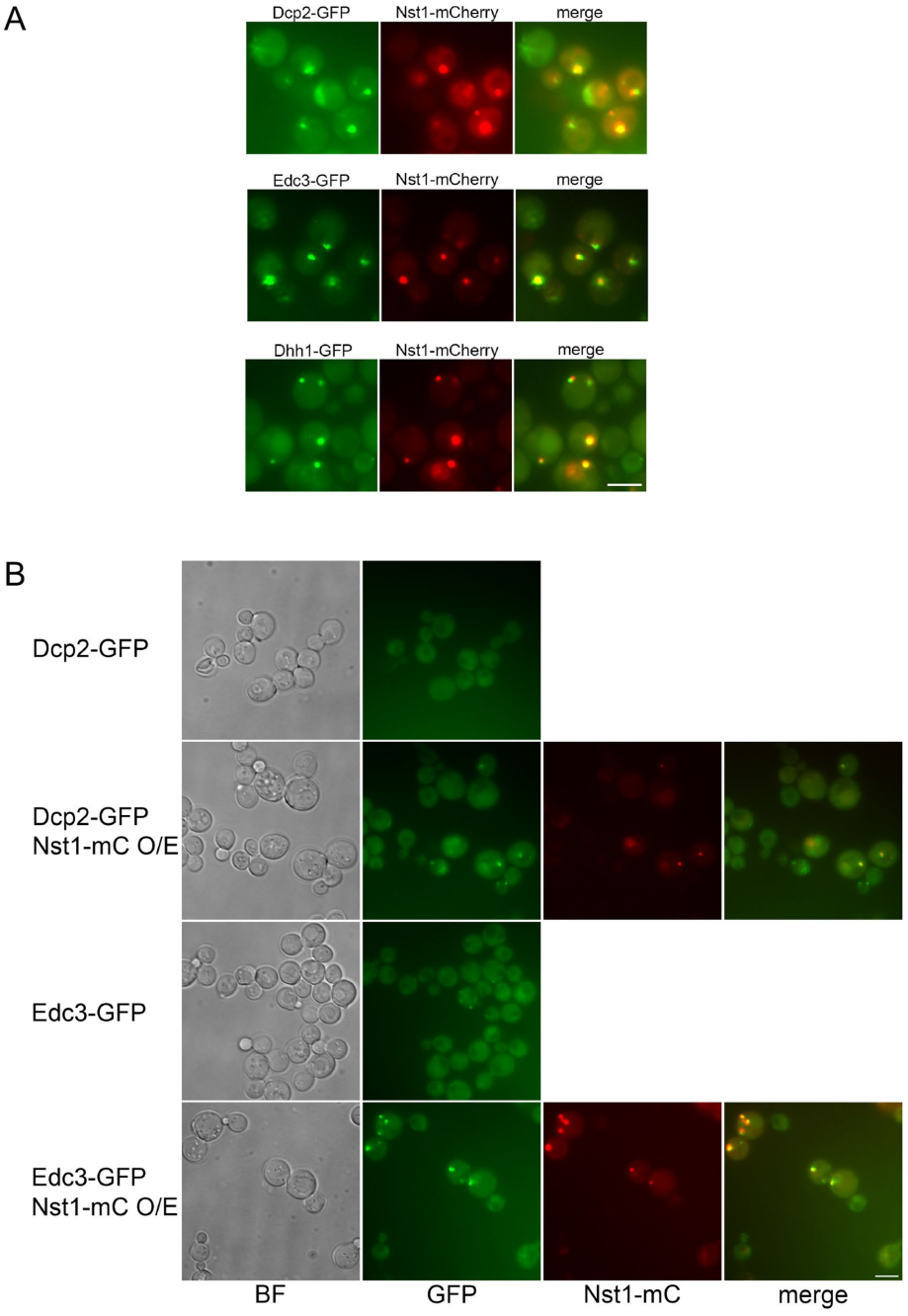

FIGURE 6: Overexpressed Nst1 colocalizes with P-body components and induces P-body assembly. (A) Colocalization studies with endogenous P-body components when Nst1-mC is overexpressed. *DCP2-GFP*, *EDC3-GFP*, and *DHH1-GFP* strains were transformed with either p416GPD or p416GPD-NST1-mCherry. Overnight cultures were diluted to OD_{600} = 0.2 in SD-URA and grown for 5 h at 30°C. (B) Overexpressed Nst1-mCherry induces P-body assembly. *DCP2-GFP* and *EDC3-GFP* strains were transformed with either p416GPD vector or p416GPD-NST1-mCherry as above. Overnight cultures were diluted to OD_{600} = 0.15 in SD-URA and grown for 3 h at 30°C. BF: brightfield. Scale bar: 5 μm.

other hand, stress granule components Pab1, Pub1, and Pbp1 were mostly localized diffusely in the cytoplasm, although we did observe some weak induction of Pbp1-GFP puncta and its colocalization with overexpressed Nst1-mCherry under normal growth conditions (Supplemental Figure S9A). Interestingly, we found that while Nst1 overexpression induced P-body assembly, it did not do so by increasing the levels of P-body or stress granule components (Figure 6B; Supplemental Figure S9B). Deletion of *NST1*, on the other hand, did not obviously affect formation of P-bodies based on GFP-tagged Dcp2, Edc3, and Dhh1 staining under normal growth conditions (Supplemental Figure S9C). This was unsurprising since there are many redundancies in protein interactions facilitating P-body formation, and no one P-body component is strictly essential for P-body assembly (Teixeira and Parker, 2007).

To determine if Nst1 is a bona fide P-body component, we fused the sequence for enhanced GFP (eGFP) to the endogenous *NST1* gene. We found that Nst1-eGFP was diffusely distributed in the cytoplasm under heat stress, normal growth, and glucose starvation conditions. However, Nst1-eGFP formed puncta that colocalized with Dcp2-mCherry in cultures entering stationary phase or under aeration-deficient glucose starvation conditions, suggesting that Nst1 is a P-body component that localizes to the P-body under specific stress conditions (Figure 7).

The serine-rich region of Nst1 is important for its localization to P-bodies

As previously noted, truncation of Nst1 beyond the serine-rich region from the C-terminal end eliminates its ability to suppress the temperature sensitivity of *nas6Δ rpn14Δ* cells (Figure 1E). We overexpressed and tracked the mCherry-tagged Nst1 truncation mutants in a Dcp2-GFP-expressing strain by fluorescence microscopy. C-terminal truncations that removed the serine-rich region from the C-terminal end were inhibited in their ability to form puncta and were diffusely localized in the cytoplasm (Figure 8). This finding revealed the importance of this serine-rich region in localizing the protein to P-bodies. Notably, the $Nst1_{440\text{-}1240}$ and $Nst1_{165\text{-}1240}$ N-terminal truncations, as well as the Nst1-W103A mutant, were still able to localize to P-bodies (Figure 8) even though these mutants also could no longer rescue *nas6Δ rpn14Δ* growth (Figure 1E); this indicates that the N-terminal region, which includes the Nst1 domain, is functionally important but is not required for its localization to P-bodies.

Nst1 overexpression inhibits global protein synthesis

A recent study found that cycloheximide treatment of *nas6Δ rpn14Δ* under heat stress inhibited cytosolic Rpt aggregates and restored proteasome assembly in this mutant (Nahar *et al.*, 2019). Aggregation of other proteins has been shown to be initiated and driven by active translation of the proteins; translational inhibition by treatment with cycloheximide inhibits their aggregation (Zhou *et al.*, 2014).

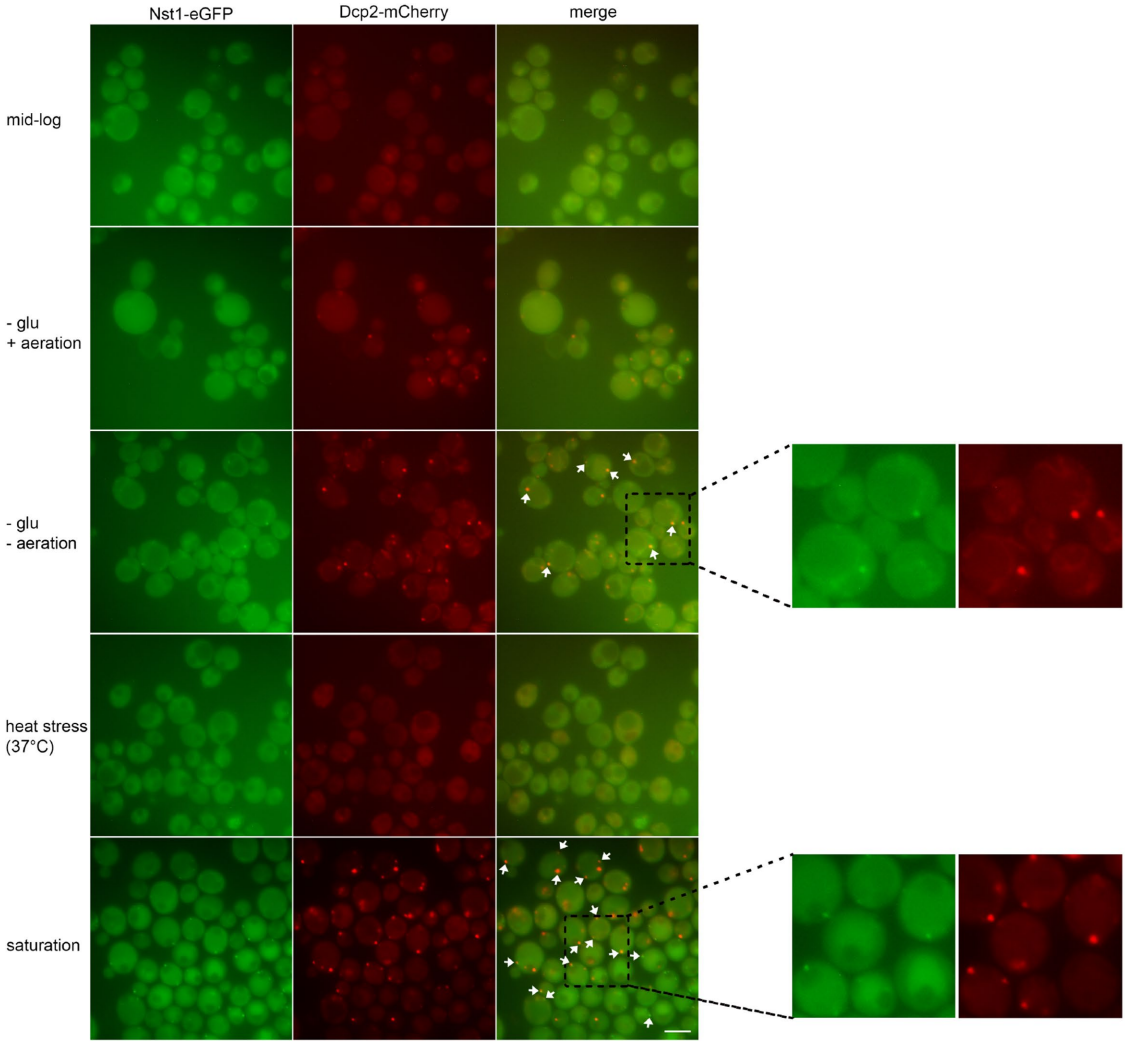

FIGURE 7: Endogenous Nst1 localizes to P-bodies under specific growth conditions. Localization of endogenous Nst1-eGFP and Dcp2-mCherry under various conditions. Overnight culture was diluted to OD_{600} = 0.15 in SD complete medium, grown for 3 h at 30°C, and imaged at midexponential stage. For the glucose starvation condition, half of the same culture grown for 3 h was harvested and washed once and grown for 10 min in SD complete medium lacking glucose either in a flask with shaking (for +aeration sample) or aliquoted into an Eppendorf tube and left to sit on the rack for 10 min (for –aeration sample) at 30°C. Aeration-deficient (–aeration) sample prepared for imaging was left on a glass slide under a coverslip for another 10 min at room temperature prior to imaging. For cultures grown to saturation, the above diluted culture in SD complete medium was grown ~24 h and then imaged. For the heat stress sample, an overnight culture was diluted to OD_{600} = 0.2 in SD complete medium and grown for 2 h at 30°C followed by 3 h at 37°C. Arrows highlight colocalization of endogenous Nst1-eGFP and Dcp2-mCherry puncta. Scale bar: 5 μm.

Therefore, we speculated that Nst1 overexpression rescues growth, aggregation, and proteasome assembly defects in RP base mutants through translational repression. Overexpression of translation-repressing P-body components such as Pat1 and Dhh1 induces growth defects in WT strains (Coller and Parker, 2005). Similarly, we found that overexpression of Nst1 caused toxicity in WT cells, in contrast to its relative salutary effect on *nas6*Δ *rpn14*Δ temperature sensitivity (Figure 9A; also see Figure 1, A and B). To determine if Nst1 overexpression represses global protein translation, we pulse-labeled cells with [^{35}S]-methionine/cysteine for short periods of time to track incorporation of the radiolabeled amino acids into newly synthesized proteins to allow for determination of global relative protein translation rates. Consistent with our hypothesis, we found that overexpression of Nst1 in *nas6*Δ *rpn14*Δ substantially inhibited rates of protein synthesis (Figure 9B; Supplemental Table S1).

Overexpression of other P-body proteins suppresses *nas6*Δ*rpn14*Δ growth defects and aggregation of Rpt subunits

Several known P-body components were also able to suppress the growth defects of *nas6*Δ *rpn14*Δ, *rpt2,5PA*, and *cim3-1* mutants (Figure 9C). Interestingly, overexpression of distinct components only suppressed a subset of the three base mutants analyzed. For instance, Edc3 overexpression suppressed only *nas6*Δ *rpn14*Δ, while Dhh1 overexpression suppressed both *nas6*Δ *rpn14*Δ and *rpt2,5PA* but not the *cim3-1* mutant. Understanding the basis of these differential effects will require further investigation.

We tracked GFP-Rpt6 puncta formation in *nas6*Δ *rpn14*Δ cells overexpressing several of these newly identified suppressors. A slight decrease was observed in numbers of GFP-Rpt6 aggregates in the mutant overexpressing Edc1 or Dhh1, while a more substantial

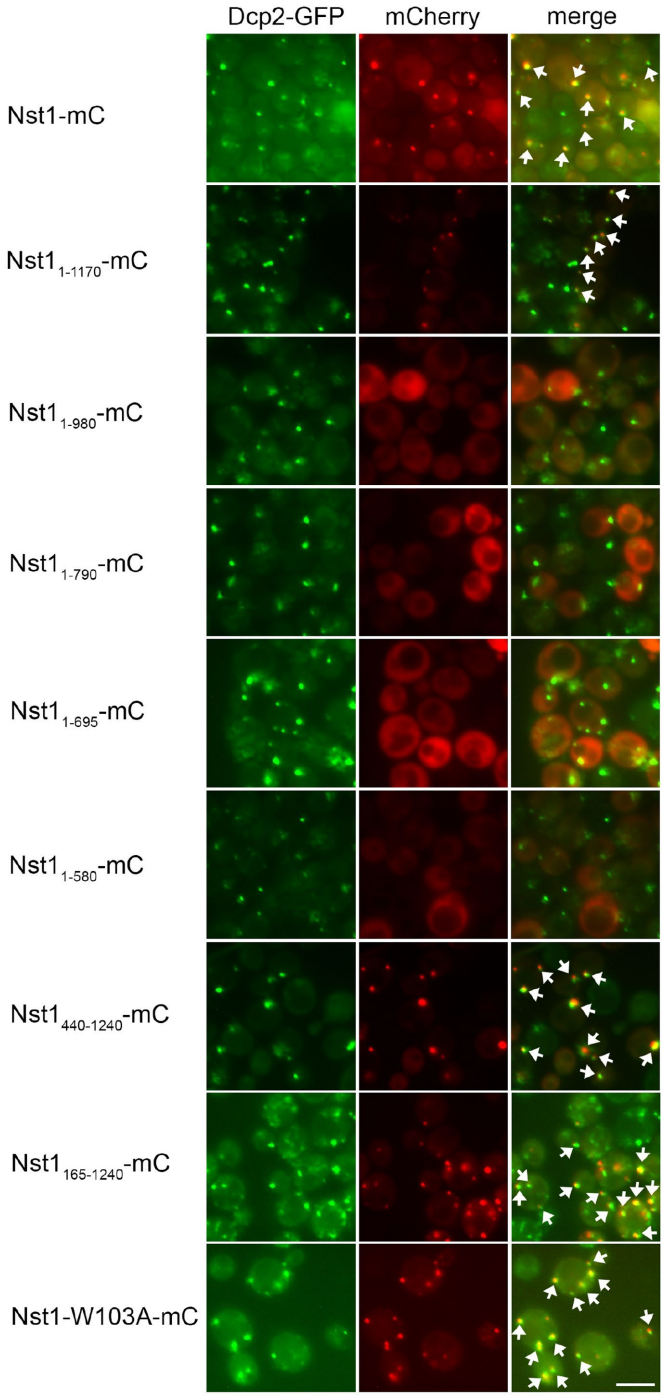

FIGURE 8: C-terminal serine-rich region of Nst1 is important for its localization to P-bodies. Analysis of Nst1 truncation mutant localization was done in a *DCP2-GFP* strain transformed with p416GPD plasmids overexpressing the indicated Nst1 constructs bearing the C-terminal mCherry tag. Cultures were grown as in Figure 6A. Arrows highlight colocalization of overexpressed Nst1-mCherry and endogenous Dcp2-GFP puncta. Note that $Nst1_{1-1170}$ is expressed at lower than WT levels (Figure 1F), but colocalization of the weaker signal with Dcp2-GFP is still observed. Scale bar: 5 μm.

decrease was seen when the mutant overexpressed Edc3 or Psp2, similar in degree to what was observed with Nst1 overexpression (Figure 9, D and E). Interestingly, our growth analysis showed that Edc1 was the strongest suppressor of *nas6Δ rpn14Δ* temperature sensitivity (Figure 9C), but the reduction in GFP-Rpt6 aggregates with Edc1 overexpression is not as pronounced as that seen with overexpression with Nst1, Edc3, or Psp2. It is possible that the mechanism by which Edc1 overexpression rescues *nas6Δ rpn14Δ* temperature sensitivity differs from that of Nst1, Edc3, and Psp2 overexpression.

Analysis of genetic interactions between *edc3Δ* and *nas6Δ rpn14Δ* at restrictive temperatures suggested that Edc3 may be important in maintaining proper base assembly under heat stress in base mutants (Supplemental Figure S10A). Less pronounced but reproducible synthetic growth defects at elevated temperatures were observed when either *dhh1Δ* or *edc1Δ* was combined with *nas6Δ rpn14Δ* (Supplemental Figure S10, A and B). We also tested whether Nst1 requires any of these P-body components for its function. Edc3 plays a major role in P-body assembly, while Dhh1 is an mRNA decapping and translational regulator that was reported to bind many mRNAs (including *NST1*) based on high-throughput studies (Coller and Parker, 2005; Decker *et al.*, 2007; Jungfleisch *et al.*, 2017; Miller *et al.*, 2018). We tested if Edc1, Edc,3 or Dhh1 was required for Nst1-mediated suppression of *nas6Δ rpn14Δ* by investigating the effect of Nst1 overexpression on temperature sensitivity of the corresponding triple mutant strains. Interestingly, we found that Nst1 overexpression was still able to suppress temperature sensitivity of *nas6Δ rpn14Δ edc3Δ* and *nas6Δ rpn14Δ edc1Δ* but not *nas6Δ rpn14Δ dhh1Δ* (Figure 9F). *DHH1* deletion, however, did not seem to affect the ability of overexpressed Nst1-mC to form puncta (Figure 9G). These findings suggest that Dhh1 is required for the function but not the localization of Nst1, analogous to what we had observed with N-terminal mutations of Nst1.

DISCUSSION

Here we have identified Nst1 as a specific suppressor of the temperature sensitivity and proteasome assembly defects caused by proteasome RP base and RAC mutations. This appears to be related to the ability of Nst1 overexpression to inhibit aggregation and cytosolic puncta formation by Rpt subunits based on analysis in the *nas6Δ rpn14Δ* base assembly mutant under heat stress. Overexpressed Nst1 itself also forms cytosolic foci that are not physically linked to Rpt puncta but instead colocalize with P-body components. Endogenous Nst1 localized to P-bodies under certain nutrient stress conditions. This condition-specific localization of Nst1 along with its low abundance may explain why Nst1 was not identified in a previous proteomics analysis of yeast P-bodies (Cary *et al.*, 2015). Congruent with its ability to drive P-body formation, Nst1 overexpression inhibited global protein synthesis, potentially by sequestering mRNAs from the active translation machinery. Insofar as chemical inhibition of protein translation is known to block aggregation of Rpt subunits in the *nas6Δ rpn14Δ* mutant under heat stress (Nahar *et al.*, 2019), this P–body-linked effect of Nst1 overexpression is likely responsible for the suppression of RP base assembly defects and Rpt subunit aggregation.

The C-terminal serine-rich region of Nst1, which is predicted to be disordered, is essential for its ability to localize to P-bodies. Notably, phosphorylation and dephosphorylation of the intrinsically disordered and serine-rich MEG-1 and MEG-3 proteins in *Caenorhabditis elegans* have been found to be important for the regulation of RNA granule assembly and disassembly (Wang *et al.*, 2014). It remains to be seen if the ability of Nst1 to promote P-body formation is regulated by phosphorylation of the serine-rich region; it is known to be phosphorylated at Ser residues here and elsewhere in the protein (Albuquerque *et al.*, 2008; Holt *et al.*, 2009;

Swaney *et al.*, 2013; Lanz *et al.*, 2021). In addition, the Nst1 serine-rich region appears to be important for the regulation of its expression since removal of this region dramatically increases its levels. This may also be true for the N-terminal region of Nst1 as deletion of its first 165 residues also leads to greatly increased levels of the protein, but this defective variant still localizes to P-bodies (Figures 2, E and F, and 8). Based on these findings, we speculate that *NST1* expression levels are regulated by the Nst1 product; this negative feedback might involve translational inhibition and sequestration of *NST1* mRNA into P-bodies, or it may reflect increased proteasomal turnover of Nst1 due to its enhancement of proteasome assembly (or both).

Our sequence analysis of the conserved Nst1 domain revealed that Nst1 orthologs are more widely distributed phylogenetically than previously reported (Goossens *et al.*, 2002). While the distribution might suggest that an Nst1-like protein was present in the last eukaryotic common ancestor, lateral gene transfer cannot be discounted and is likely in several examples. The ~60-residue "Nst1 domain" and its most conserved residue, Trp103, are necessary for the ability of Nst1 to suppress the temperature sensitivity of *nas6*Δ *rpn14*Δ, highlighting the importance of this domain for Nst1 function. Structural modeling suggests the Nst1 domain has structural similarity to the redox-regulated Hsp33 molecular chaperone in bacteria with conservation of three of four critical cysteines. Interestingly, we found that *nst1*Δ strain is highly sensitive to oxidative stress caused by diamide, although the conserved cysteines in the Nst1 domain do not appear to contribute to diamide resistance. Further experiments on the role of Nst1 in conferring tolerance to diamide should nevertheless be illuminating.

Our study showed that overexpression of P-body components other than Nst1 can also suppress the temperature sensitivity of base assembly mutants. Dhh1 overexpression had previously been reported to inhibit global protein translation, and we have found that overexpression of Dhh1 also suppresses the temperature sensitivity of *nas6*Δ *rpn14*Δ and *rpt2,5PA* but not of *cim3-1* (*rpt6-1*) (Coller and Parker, 2005). Interestingly, Dhh1 overexpression seemed to exacerbate the growth defect of *cim3-1* cells. A potential explanation for this is that translation repression is generally toxic, and the degree of proteasome assembly rescue in each mutant and the relative benefit of that rescue to growth may be different for each base mutant. Additionally, fully assembled proteasomes in *cim3-1* remain defective for activity (Ghislain *et al.*, 1993).

Interestingly, Edc3 and Psp2 are not known to be translational repressors but are reported to be important in P-body assembly (Decker *et al.*, 2007; Rao and Parker, 2017). Their ability to suppress *nas6*Δ *rpn14*Δ temperature sensitivity and Rpt6 aggregation when overexpressed suggests they may also enhance translation repression, whether directly or indirectly, or that induction of P-body assembly could make additional contributions to the suppression seen with RP base assembly mutants.

High-throughput data suggest that Nst1 physically interacts with several components of the P-body such as Lsm4 and the Ccr4-Not complex (Fromont-Racine *et al.*, 2000; Uetz *et al.*, 2000; Tarassov *et al.*, 2008; Schlecht *et al.*, 2012). These findings further support localization of Nst1 to P-bodies. Interestingly, we found that *DHH1* deletion abrogates the ability of Nst1 to suppress the temperature sensitivity of *nas6*Δ *rpn14*Δ cells. This suggests that the Dhh1 RNA helicase might mediate the activity of Nst1. Many components of P-bodies, including Dhh1, directly interact with mRNAs (Luo *et al.*, 2018). It remains to be investigated whether Nst1 binds mRNA directly. Given that endogenous Nst1 localizes to P-bodies in cultures under saturating and aeration-dependent glucose starvation conditions, we propose that Nst1 functions as a stress-response protein that helps sequester mRNAs in P-bodies to control their translational availability.

No previous work had connected proteasome assembly to the P-body. Assembly of the nine-subunit RP base might be particularly sensitive to imbalances between some of its intermediates, which might arise in conditions such as those mentioned above. This is predicted to cause aggregation of Rpt subunits or accumulation of other dead-end intermediates that slow full proteasome formation. Counteracting this, increases in Nst1 levels or its promotion of P-body formation could selectively dampen protein translation in a way that restores balanced expression of different subunits or subcomplexes of multiprotein complexes such as the proteasome RP. Our evidence for this has mostly come from analysis of cells with mutated RP base subunits or missing RP assembly factors and forced overexpression of Nst1. It will be important to determine if the Nst1 protein or other P-body components that stimulate P-body formation under particular physiological stresses can promote proper assembly of specific protein complexes, including that of the proteasome, through such a translation-dependent rebalancing of assembly intermediates.

MATERIALS AND METHODS

Yeast strains

Yeast strains were made and manipulated according to standard protocols (Guthrie and Fink, 2002). Yeast strains and plasmids used in this study are listed in Supplemental Tables S2 and S3, respectively.

High-copy suppressor screen

The *rpt2,5PA* mutant strain was grown in YPD at 30°C overnight. The next day, tiled yeast genomic DNA library plasmids (Jones *et al.*, 2008) that were pooled into 17 sublibraries were transformed into *rpt2,5PA* cells, plated onto 17 selective defined (SD)-Leu+4 μM canavanine plates, and incubated at 35.5°C. Colony formation was monitored over the next 2–3 d. Because many colonies were found on plates where *rpt2,5PA* was transformed with pooled sublibrary plasmids that included the *RPT2* and *RPT5* genes, only a few colonies were picked from these plates. Colonies grown on each plate were isolated and grown in YPD at 30°C overnight. The next day, suppressor plasmids along with genomic DNA were isolated via a previously described protocol (Hoffman and Winston, 1987). Isolated DNA from the yeast colonies was transformed into *TOP10F'* electrocompetent cells and plated onto LB + Amp plates. The suppressor plasmids were then isolated using QIAprep Spin Miniprep Kit (Qiagen) and the insert ends were subsequently identified via DNA sequencing and mapped to the ordered genomic library. The high-copy suppressor screen was conducted in duplicate, and the combined suppressors identified from both screens are listed in Table 1. Plasmids that yield very weak (but reproducible) suppression were not pursued further.

Yeast growth assay and suppression analysis

For spot assays, yeast strains were grown in YPD-rich medium or SD media with defined nutrient dropouts at 30°C overnight to saturation. The next day, cultures were diluted to OD_{600} = 0.2 in sterile water. Cells were spotted onto plates in sixfold decreasing concentrations. Plates were then incubated at various temperatures and for the number of days indicated in the figures.

Nondenaturing gel analyses of yeast extracts

Yeast extracts prepared for nondenaturing gel analyses were prepared as previously described with minor modifications

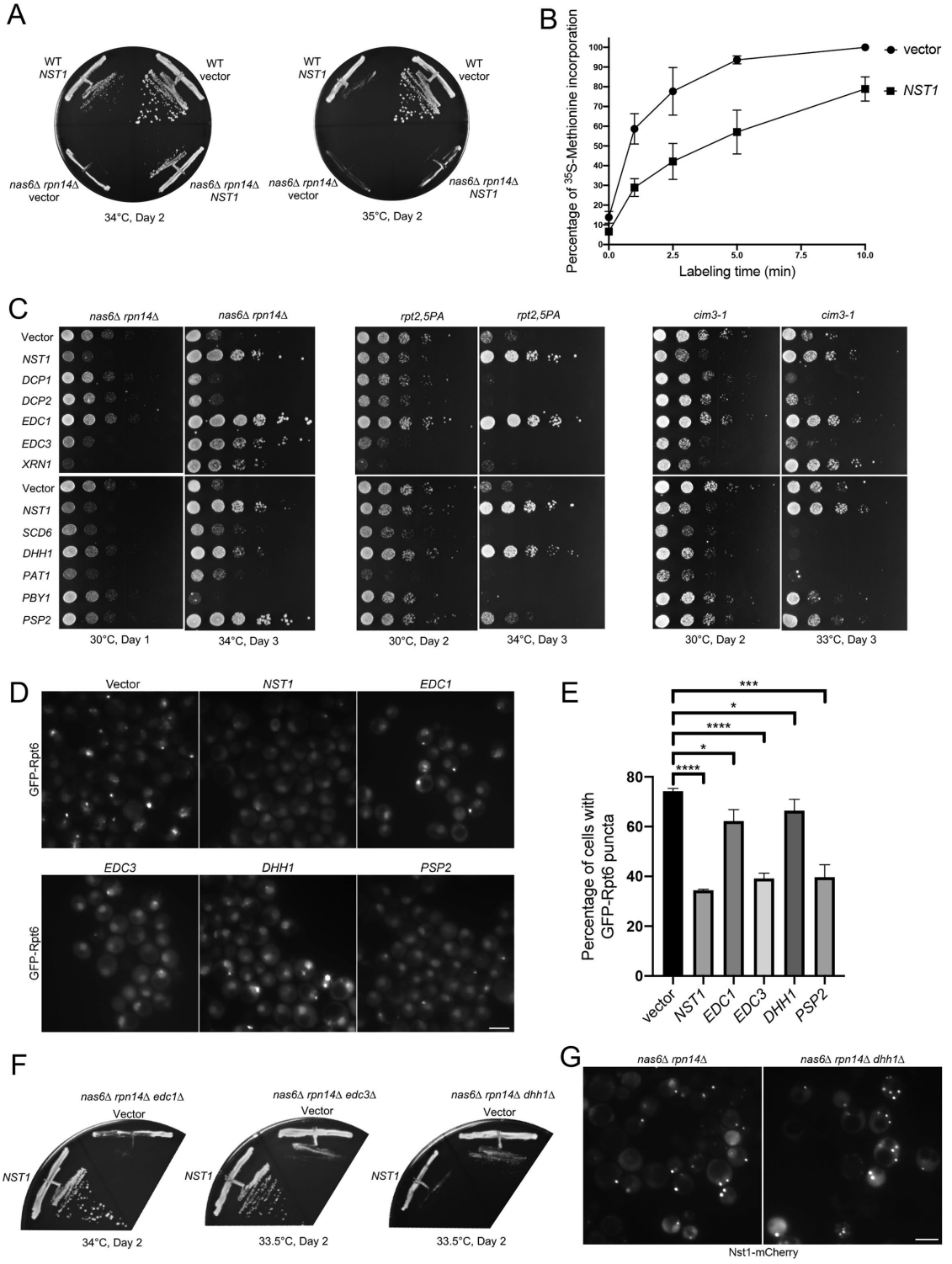

FIGURE 9: Overexpression of other P-body components in *nas6Δ rpn14Δ* cells suppresses temperature sensitivity and Rpt6 aggregation. (A) Differential effect of Nst1 overexpression on growth of WT and *nas6Δ rpn14Δ* strains. Strains were transformed with either p426GPD or p426GPD-NST1. Streak tests were conducted on SD-URA plates. (B) [^{35}S]-Met/Cys pulse-labeling assay measuring the effect of Nst1 overexpression on overall protein synthesis. The *nas6Δ rpn14Δ* strain was transformed with either p426GPD or p426GPD-NST1. For normalization of each replicate, the TCA-insoluble [^{35}S]-Met/Cys amount (CPM) at 10 min for cells transformed with the p426GPD vector was designated as 100% incorporation. Mean ± SD from three independent transformants for each plasmid. (C) Effect of overexpression of various P-body proteins on temperature sensitivity of *nas6Δ rpn14Δ*, *rpt2,5PA*, and *cim3-1*. All P-body constructs were cloned into p416GPD and transformed into the aforementioned mutants. Spot assays were conducted on SD-URA plates. (D) Overexpressed P-body proteins that suppressed ts growth in C were tested for GFP-Rpt6 puncta formation in *nas6Δ rpn14Δ*. Cells with chromosomal *GFP-RPT6* were transformed with p416GPD, p416GPD-NST1,

(Kusmierczyk *et al.*, 2008). Yeast strains were grown in YPD or SD media at 30°C overnight. For analysis of the effects of Nst1 overexpression (Nst1 expressed under its native promoter in pRS316) on proteasome assembly in WT versus *rpt2,5PA* strains, overnight cultures were diluted to OD_{600} = 0.05 in SD-URA and grown at 36°C to exponential phase. Other analyses were conducted by diluting overnight cultures to OD_{600} = 0.2 and grown until midexponential phase at the temperatures noted in the figure legends. Cultures were harvested, washed with sterile cold water, flash-frozen in liquid nitrogen, and stored at –80°C. Frozen cells were ground with consistently chilled mortar and pestle (with liquid nitrogen) until a fine powder was formed. The powder was then dissolved in proteasome extraction buffer (50 mM Tris-HCl, pH 7.5; 5 mM $MgCl_2$, 10% glycerol, 5 mM ATP) for 10 min with occasional vortexing and incubation on ice between each vortex run. To remove unlysed cells and cell debris, samples were centrifuged at 22,000 × *g* for 10 min and resulting supernatants were transferred into a fresh tube. Samples were centrifuged again at 22,000 × *g* for 5 min to further clarify the supernatant. The supernatants were subjected to BCA assays (Thermo Fisher Scientific) to determine protein concentration; 50 µg total protein for each sample were run through nondenaturing gels. Gels were subjected to either Suc-LLVY-AMC (Sigma-Aldrich) fluorogenic substrate overlay assays or native immunoblot analyses. The procedure for the substrate overlay assay was described previously (Li *et al.*, 2015). For analyses of steady-state levels of soluble proteasome subunits (Supplemental Figure S5A), equal amounts of protein from each sample were loaded onto a denaturing gel and subjected to immunoblot analyses.

Denaturing gel analyses of total protein in yeast extracts

Yeast extracts for denaturing gel analyses were prepared based on a previously described protocol with slight modifications (Kushnirov, 2000). For analysis of total protein (both soluble and insoluble proteins) of each sample, cells corresponding to 2.5 OD_{600} units of cultures were harvested and washed with sterile water. Samples were then resuspended in 200 µl sterile water followed by 200 µl of 0.2M NaOH and incubated at room temperature for 5 min with intermittent vortexing. Next, samples were centrifuged at 10,000 × *g* for 1 min and the supernatant was discarded. The samples were then resuspended in 100 µl 1× SDS sample buffer containing 4% β-mercaptoethanol (BME) and boiled at 100°C for 5 min followed by recentrifugation at 10,000 × *g* for 1 min; 10–15 µl of the supernatants were loaded onto denaturing gels.

Immunoblotting and antibodies

To detect proteins by immunoblotting, samples run in denaturing or nondenaturing gels were transferred to PVDF membranes (Millipore). The following primary antibodies were used in this study: anti-α4/Pre6 (D. Wolf), anti-Rpt1 (Enzo Life Sciences), anti-Rpt2 (Enzo Life Sciences), anti-Rpt3 (Enzo Life Sciences), anti-Rpt4 (W. Tansey), anti-Rpt5 (Enzo Life Sciences), anti-Rpt6 (C. Mann), anti-Rpn12 (D. Finley), anti-Hsm3, anti-Nas2, and anti-Nas6 (all Hochstrasser lab stocks; Funakoshi *et al.*, 2009); anti-FLAG (Sigma-Aldrich), anti-GFP/JL8 (TaKaRa), and Pgk1 (Invitrogen). Secondary antibodies used for enhanced chemiluminescence were anti-mouse IgG, horseradish peroxidase (HRP)-linked (from sheep) and anti-Rabbit IgG, HRP-linked (from donkey) (both GE Healthcare).

qPCR analysis of proteasome subunit and chaperone transcript levels

For analysis of proteasome subunit and chaperone transcript levels, cells corresponding to one OD_{600} unit of cultures were harvested and washed with sterile water. Total RNA from each sample was extracted using RNeasy Mini Kit (Qiagen) and eluted in 50 µl nuclease-free water. DNA from each sample was removed using a DNA-*free* Kit (Ambion). The iScript cDNA Synthesis Kit (Bio-Rad) was used to reverse transcribe the RNA into cDNA. The cDNA of each gene analyzed was quantified using iQ SYBR Green Supermix (Bio-Rad) on a LightCycler480 instrument (Roche). All experiments were conducted according to manufacturers' protocols.

Yeast protein aggregation assay

Yeast strains in Figure 4C were grown in SD-URA at 30°C overnight. The next day, the cultures were diluted to OD_{600} = 0.2 in SD-URA for 2 h at 30°C followed by another 3 h at 37°C. Cultures were harvested, washed with sterile cold water, flash-frozen with liquid nitrogen, and stored at –80°C. Frozen cells were ground with liquid nitrogen-chilled mortar and pestle until a fine powder was formed. The powder was transferred into a prechilled 1.5-ml Eppendorf tube and resuspended in ice-cold lysis buffer (50 mM Tris, pH 7.5; 150 mM NaCl, 1% glycerol, 1 mM EDTA, 1 mM PMSF, 1× EDTA-free cOmplete Protease Inhibitor Cocktail; Roche) and vortexed intermittently for 10 min with incubation on ice between each vortex run. The samples were centrifuged at 3000 × *g* for 30 s to remove unlysed cells and cell debris. The resulting supernatant was transferred into a fresh tube. Protein concentration of each sample was determined via BCA assay (Thermo Fisher Scientific). Protein concentrations were then normalized across all samples by diluting samples with lysis buffer. An aliquot of each sample was set aside as total protein (T). Next, equal volumes of samples were subjected to ultracentrifugation at 100,000 × *g* for 20 min using a Beckman Coulter TLA-55 rotor. The supernatants (S) were transferred into a fresh tube. The remaining pellets were washed with lysis buffer and subjected to another run of ultracentrifugation at 100,000 × *g* for 20 min. The supernatants were discarded, and the pellets were resuspended with half the volume of supernatant and designated (P). (T), (S), and (P) samples were brought to 1× concentration of SDS sample buffer containing 1% BME (final). The samples were then boiled at 100°C for 5 min. Samples were subsequently centrifuged at 10,000 × *g* for 1 min. Equal volumes of (T), (S), and (P) were loaded onto nondenaturing gels and subjected to immunoblot analyses. The concentration of P sample loaded was therefore twice of those of T and S.

p416GPD-EDC1, p416GPD-EDC3, p416GPD-DHH1, or p416GPD-PSP2. Overnight cultures were diluted to OD_{600} = 0.2 in SD-URA and grown for 2 h at 30°C followed by 3 h at 37°C. GFP-Rpt6 distribution examined by fluorescence microscopy. Scale bar, 5 µm. (E) Quantification of GFP-Rpt6 puncta in (D). Mean ± SD from three independent transformants for each plasmid. More than 200 cells were analyzed for each isolate. Unpaired *t* test: **P* < 0.05; ****P* < 0.001; *****P* < 0.0001. (F) Effect of Nst1 overexpression on temperature sensitivity of the indicated triple mutants. *S*trains were transformed with either p416GPD or p416GPD-NST1. Streak tests were conducted on SD-URA plates. (G) Localization of overexpressed Nst1-mCherry in *nas6*Δ *rpn14*Δ and *nas6*Δ *rpn14*Δ *dhh1*Δ. Strains were transformed with p416GPD-NST1-mCherry. Overnight cultures were diluted to OD_{600} = 0.2 in SD-URA and grown for 2 h at 30°C followed by 3 h at 37°C. Scale bar: 5 µm.

Yeast fluorescence microscopy

Starter cultures were grown either in SD-URA or in SD complete medium at 30°C overnight. The next day, cultures were diluted in fresh medium and grown for the length of time and temperature specified in the figure legends. Visualization and image processing of fluorescent proteins in yeast were conducted as described (Li *et al.*, 2019). Briefly, yeast cultures were visualized using an Axioskop fluorescence microscope (Carl Zeiss) equipped with a plan-Apochromat 100×/1.40 oil DIC objective lens, an AxioCam MRm CCD Camera (Carl Zeiss), and a HBO100W/2 light source. Microscopy images were captured using AxioVision software and processed using Adobe Photoshop.

[^{35}S]-Methionine/cysteine pulse-labeling

A *nas6*Δ *rpn14*Δ strain transformed with either p426GPD or p426GPD-NST1 was grown in SD-URA at 30°C overnight. The next day, cultures were diluted to OD_{600} = 0.2 and grown for 4.5 h at 30°C; 12.5 OD_{600} units of cells were then harvested at 5000 rpm for 5 min. The cells were washed twice with 1 ml SD-URA-MET preincubated at 30°C and centrifuged at 10,000 rpm for 2 min. The cells were then resuspended in 550 µl of SD-URA-MET; 20 µl (~220 µCi) of [^{35}S]-Met/Cys label (PerkinElmer) were mixed into the sample; 100 µl aliquots were immediately removed, and protein synthesis was quenched by the addition to 100 µl 2× SDS lysis buffer (2% SDS, 90 mM HEPES, pH 7.5; 30 mM DTT) on ice. These samples were the 0-min time point samples. The remainder of each culture was left at 30°C, and 100 µl samples were removed at the time points listed in the figure and quenched as above. All quenched samples were boiled in a 100°C water bath for 8 min and centrifuged at 10,000 rpm for 2 min; 10 µl supernatant for each time point was spotted onto chromatography paper (Fisher Scientific) and left to dry at room temperature for 15 min. The dried filter with the extracts spotted onto it was washed twice in room temperature in 10% trichloroacetic acid (TCA), followed by boiling in 10% TCA for 5 min, and washing twice again at room temperature in 10% TCA. The blotted paper was subsequently washed twice in 100% ethanol and left to dry under a heat lamp for 15 min. The dried filter was cut into individual sample squares and incubated in liquid scintillation cocktail (Opti-Fluor, PerkinElmer) for 30 min at room temperature. [^{35}S]-Met/Cys incorporation was counted using a liquid scintillation counter.

ACKNOWLEDGMENTS

We thank Carolyn Breckel, Jianhui Li, and Mengwen Zhang for critical reading of the manuscript. We are grateful to Soyeon Park for providing yeast strains and Dan Finley, Carl Mann, Bill Tansey, and Dieter Wolf for providing antibodies used in this study. This work is supported by National Institutes of Health grants (GM136325 and GM083050) to M.H.

REFERENCES

Albuquerque CP, Smolka MB, Payne SH, Bafna V, Eng J, Zhou H (2008). A multidimensional chromatography technology for in-depth phosphoproteome analysis. Mol Cell Proteomics 7, 1389–1396.

Bard JAM, Goodall EA, Greene ER, Jonsson E, Dong KC, Martin A (2018). Structure and function of the 26S proteasome. Annu Rev Biochem 87, 697–724.

Boeynaems S, Alberti S, Fawzi NL, Mittag T, Polymenidou M, Rousseau F, Schymkowitz J, Shorter J, Wolozin B, Van Den Bosch L, *et al.* (2018). Protein phase separation: a new phase in cell biology. Trends Cell Biol 28, 420–435.

Budenholzer L, Cheng CL, Li Y, Hochstrasser M (2017). Proteasome structure and assembly. J Mol Biol 429, 3500–3524.

Cary GA, Vinh DB, May P, Kuestner R, Dudley AM (2015). Proteomic analysis of Dhh1 complexes reveals a role for Hsp40 chaperone Ydj1 in yeast P-body assembly. G3 (Bethesda) 5, 2497–2511.

Cheng CL, Wong MK, Li Y, Hochstrasser M (2021). Conserved proline residues in the coiled coil-OB domain linkers of Rpt proteins facilitate eukaryotic proteasome base assembly. J Biol Chem 296, 100660.

Coller J, Parker R (2005). General translational repression by activators of mRNA decapping. Cell 122, 875–886.

Decker CJ, Parker R (2012). P-bodies and stress granules: possible roles in the control of translation and mRNA degradation. Cold Spring Harb Perspect Biol 4, a012286.

Decker CJ, Teixeira D, Parker R (2007). Edc3p and a glutamine/asparagine-rich domain of Lsm4p function in processing body assembly in Saccharomyces cerevisiae. J Cell Biol 179, 437–449.

Fromont-Racine M, Mayes AE, Brunet-Simon A, Rain JC, Colley A, Dix I, Decourty L, Joly N, Ricard F, Beggs JD, Legrain P (2000). Genome-wide protein interaction screens reveal functional networks involving Sm-like proteins. Yeast 17, 95–110.

Funakoshi M, Tomko RJ Jr, Kobayashi H, Hochstrasser M (2009). Multiple assembly chaperones govern biogenesis of the proteasome regulatory particle base. Cell 137, 887–899.

Ghislain M, Udvardy A, Mann C (1993). S. cerevisiae 26S protease mutants arrest cell division in G2/metaphase. Nature 366, 358–362.

Goossens A, Forment J, Serrano R (2002). Involvement of Nst1p/YNL091w and Msl1p, a U2B″ splicing factor, in Saccharomyces cerevisiae salt tolerance. Yeast 19, 193–202.

Guthrie C, Fink GR (2002). Guide to yeast genetics and molecular biology. Methods Enzymol 194, 3–933.

Hanssum A, Zhong Z, Rousseau A, Krzyzosiak A, Sigurdardottir A, Bertolotti A (2014). An inducible chaperone adapts proteasome assembly to stress. Mol Cell 55, 566–577.

Hoffman CS, Winston F (1987). A ten-minute DNA preparation from yeast efficiently releases autonomous plasmids for transformation of Escherichia coli. Gene 57, 267–272.

Holt LJ, Tuch BB, Villén J, Johnson AD, Gygi SP, Morgan DO (2009). Global analysis of Cdk1 substrate phosphorylation sites provides insights into evolution. Science 325, 1682–1686.

Jones GM, Stalker J, Humphray S, West A, Cox T, Rogers J, Dunham I, Prelich G (2008). A systematic library for comprehensive overexpression screens in Saccharomyces cerevisiae. Nat Methods 5, 239–241.

Ju D, Wang L, Mao X, Xie Y (2004). Homeostatic regulation of the proteasome via an Rpn4-dependent feedback circuit. Biochem Biophys Res Commun 321, 51–57.

Jungfleisch J, Nedialkova DD, Dotu I, Sloan KE, Martinez-Bosch N, Brüning L, Raineri E, Navarro P, Bohnsack MT, Leidel SA, Díez J (2017). A novel translational control mechanism involving RNA structures within coding sequences. Genome Res 27, 95–106.

Kaneko T, Hamazaki J, Iemura S, Sasaki K, Furuyama K, Natsume T, Tanaka K, Murata S (2009). Assembly pathway of the mammalian proteasome base subcomplex is mediated by multiple specific chaperones. Cell 137, 914–925.

Kelley LA, Mezulis S, Yates CM, Wass MN, Sternberg MJ (2015). The Phyre2 web portal for protein modeling, prediction and analysis. Nat Protoc 10, 845–858.

Kushnirov VV (2000). Rapid and reliable protein extraction from yeast. Yeast 16, 857–860.

Kusmierczyk AR, Kunjappu MJ, Funakoshi M, Hochstrasser M (2008). A multimeric assembly factor controls the formation of alternative 20S proteasomes. Nat Struct Mol Biol 15, 237–244.

Lanz MC, Yugandhar K, Gupta S, Sanford EJ, Faça VM, Vega S, Joiner AMN, Fromme JC, Yu H, Smolka MB (2021). In-depth and 3-dimensional exploration of the budding yeast phosphoproteome. EMBO Rep 22, e51121.

Le Tallec B, Barrault MB, Guerois R, Carre T, Peyroche A (2009). Hsm3/S5b participates in the assembly pathway of the 19S regulatory particle of the proteasome. Mol Cell 33, 389–399.

Leng G, Song K (2016). Direct interaction of Ste11 and Mkk1/2 through Nst1 integrates high-osmolarity glycerol and pheromone pathways to the cell wall integrity MAPK pathway. FEBS Lett 590, 148–160.

Li J, Breker M, Graham M, Schuldiner M, Hochstrasser M (2019). AMPK regulates ESCRT-dependent microautophagy of proteasomes concomitant with proteasome storage granule assembly during glucose starvation. PLoS Genet 15, e1008387.

Li Y, Tomko RJ Jr, Hochstrasser M (2015). Proteasomes: isolation and activity assays. Curr Protoc Cell Biol 67, 3.43.41-43.43.20.

London MK, Keck BI, Ramos PC, Dohmen RJ (2004). Regulatory mechanisms controlling biogenesis of ubiquitin and the proteasome. FEBS Lett 567, 259–264.
Luo Y, Na Z, Slavoff SA (2018). P-Bodies: composition, properties, and functions. Biochemistry 57, 2424–2431.
Mannhaupt G, Schnall R, Karpov V, Vetter I, Feldmann H (1999). Rpn4p acts as a transcription factor by binding to PACE, a nonamer box found upstream of 26S proteasomal and other genes in yeast. FEBS Lett 450, 27–34.
Miller JE, Zhang L, Jiang H, Li Y, Pugh BF, Reese JC (2018). Genome-wide mapping of decay factor-mRNA interactions in yeast identifies nutrient-responsive transcripts as targets of the deadenylase Ccr4. G3 (Bethesda) 8, 315–330.
Muhlrad D, Parker R (2005). The yeast EDC1 mRNA undergoes deadenylation-independent decapping stimulated by Not2p, Not4p, and Not5p. EMBO J 24, 1033–1045.
Nahar A, Fu X, Polovin G, Orth JD, Park S (2019). Two alternative mechanisms regulate the onset of chaperone-mediated assembly of the proteasomal ATPases. J Biol Chem 294, 6562–6577.
Rao BS, Parker R (2017). Numerous interactions act redundantly to assemble a tunable size of P bodies in Saccharomyces cerevisiae. Proc Natl Acad Sci USA 114, E9569–E9578.
Roelofs J, Park S, Haas W, Tian G, McAllister FE, Huo Y, Lee BH, Zhang F, Shi Y, Gygi SP, Finley D (2009). Chaperone-mediated pathway of proteasome regulatory particle assembly. Nature 459, 861–865.
Romero P, Obradovic Z, Li X, Garner EC, Brown CJ, Dunker AK (2001). Sequence complexity of disordered protein. Proteins 42, 38–48.
Rousseau A, Bertolotti A (2016). An evolutionarily conserved pathway controls proteasome homeostasis. Nature 536, 184–189.
Saeki Y, Toh EA, Kudo T, Kawamura H, Tanaka K (2009). Multiple proteasome-interacting proteins assist the assembly of the yeast 19S regulatory particle. Cell 137, 900–913.
Schlecht U, Miranda M, Suresh S, Davis RW, St Onge RP (2012). Multiplex assay for condition-dependent changes in protein-protein interactions. Proc Natl Acad Sci USA 109, 9213–9218.
Swaney DL, Beltrao P, Starita L, Guo A, Rush J, Fields S, Krogan NJ, Villén J (2013). Global analysis of phosphorylation and ubiquitylation cross-talk in protein degradation. Nat Methods 10, 676–682.
Tarassov K, Messier V, Landry CR, Radinovic S, Serna Molina MM, Shames I, Malitskaya Y, Vogel J, Bussey H, Michnick SW (2008). An in vivo map of the yeast protein interactome. Science 320, 1465–1470.
Teixeira D, Parker R (2007). Analysis of P-body assembly in Saccharomyces cerevisiae. Mol Biol Cell 18, 2274–2287.
Thomsen MC, Nielsen M (2012). Seq2Logo: a method for construction and visualization of amino acid binding motifs and sequence profiles including sequence weighting, pseudo counts and two-sided representation of amino acid enrichment and depletion. Nucleic Acids Res 40, W281–W287.
Tomko RJ Jr, Hochstrasser M (2013). Molecular architecture and assembly of the eukaryotic proteasome. Annu Rev Biochem 82, 415–445.
Uetz P, Giot L, Cagney G, Mansfield TA, Judson RS, Knight JR, Lockshon D, Narayan V, Srinivasan M, Pochart P, *et al*. (2000). A comprehensive analysis of protein-protein interactions in Saccharomyces cerevisiae. Nature 403, 623–627.
Wang JT, Smith J, Chen BC, Schmidt H, Rasoloson D, Paix A, Lambrus BG, Calidas D, Betzig E, Seydoux G (2014). Regulation of RNA granule dynamics by phosphorylation of serine-rich, intrinsically disordered proteins in C. elegans. Elife 3, e04591.
Winter J, Jakob U (2004). Beyond transcription–new mechanisms for the regulation of molecular chaperones. Crit Rev Biochem Mol Biol 39, 297–317.
Xie Y, Varshavsky A (2001). RPN4 is a ligand, substrate, and transcriptional regulator of the 26S proteasome: a negative feedback circuit. Proc Natl Acad Sci USA 98, 3056–3061.
Zhou C, Slaughter BD, Unruh JR, Guo F, Yu Z, Mickey K, Narkar A, Ross RT, McClain M, Li R (2014). Organelle-based aggregation and retention of damaged proteins in asymmetrically dividing cells. Cell 159, 530–542.